The Effect of Mutual Coupling on the Noise Performance of Large Antenna Arrays

by

Jacki van der Merwe

Thesis presented in partial fulfilment of the requirements for the degree of Master of Science in Engineering at Stellenbosch University

Supervisor: Professor Keith Duncan Palmer
Department of Electrical and Electronic Engineering

March 2010

Declaration

By submitting this thesis electronically, I declare that the entirety of the work contained therein is my own, original work, that I am the owner of the copyright thereof (unless to the extent explicitly otherwise stated) and that I have not previously in its entirety or in part submitted it for obtaining any qualification.

March 2010

Abstract

Worldwide, more large antenna arrays are being deployed in areas of science previously dominated by other antenna geometries. Applications for large arrays include Radar, Satellite Communications and Radio Astronomy. Even though the use of large arrays solve some of the difficulties posed by more traditional antennas, new challenges are also faced. One of these challenges is the problem of noise coupling, and how the overall system performance is affected by it. The Focal Plane Array (FPA), which is a new example of a large antenna array, is currently being researched at a number of institutions worldwide for use in Radio Astronomy. As a result, FPA's were used as an example element to demonstrate the practical importance of this research.

In this study, the effect of mutual coupling on the noise performance of FPA's was illustrated. This was done by calculating the mutual coupling between the elements of the array, and then calculating the noise power received by each element as a result of the mutual coupling. Next, the *Active Noise Figure* and *Active Noise Temperature* were calculated. These parameters were introduced to visualise the effect of mutual coupling on the overall noise performance of the array.

Since FPA's are by definition large, conventional brute-force analysis techniques are very resource intensive. Solving the coupling terms using these methods therefore requires the use of computer clusters even during the design phase of the antenna, which is very expensive. A method was therefore developed to calculate the coupling terms of a large array using Periodic Boundary Conditions. The method uses infinite array analysis, which resulted in an improvement in memory usage in orders of magnitude. This improvement comfortably places the memory requirements for the analysis of large arrays within the range of current personal computers. The results also displayed a reasonable amount of accuracy for use during the design phase of an array.

The additional noise power on each element as a result of mutual coupling were also calculated. This was achieved by developing an equivalent circuit diagram that represents the system in terms of the noise and transmission parameters of the LNA of each receiver channel, and the coupling terms of the antenna array. Lastly, the active noise temperature and active noise figure are calculated. The theory was implemented by means of a script with a graphical user interface, to provide easy-to-use access to the theory. A quick reference table of estimated noise coupling penalty versus first term coupling and LNA noise temperature was also compiled.

The results of an example calculation showed a significant amount of noise coupling in an 8×8 Vivaldi array. The noise coupling resulted in an increase in system noise temperature, T_{sys}, in the order of 9% of the LNA noise temperature, T_{LNA}. According to the SKA T_{sys} budget, this results in an approximate T_{sys} increase of 1.3 Kelvin. In the context of Radio Astronomy, this additional source of noise cannot be ignored, as it can greatly affect the usebility of the telescope for certain areas of research.

Samevatting

Groot antennaskikkings word deesdae al hoe meer ingespan in plek van ander tradisionele antennamodelle. Toepassings vir groot antennaskikkings sluit Radar, Satellietkommunikasie en Radioastronomie in. Alhoewel die gebruik van groot antennaskikkings baie van die probleme wat deur ander tradisionele antennamodelle veroorsaak word oplos, word nuwe uitdagings terselfdertyd geskep. Een van hierdie nuwe uitdagins is ruiskoppelling en hoe dit die ruisgedrag van die stelsel as 'n geheel affekteer. 'n Beeldvlakskikking (FPA), is 'n opwindende nuwe voorbeeld van 'n groot antennaskikking en die moontlikheid vir die gebruik daarvan in radioastronomie word tans wêreldwyd nagevors. Om hierdie rede is die FPA gekies as voorbeeldelement om die bruikbaarheid van hierdie navorsing in die praktyk te beklemtoon.

In hierdie studie word die effek van wedersydse koppelling op die ruisgedrag van FPA's geïllustreer. Dit word gedoen deur eers die wedersydse koppelling tussen die elemente van die antennaskikking te bereken en dan die ruisdrywing wat deur elke element ontvang word as gevolg van wedersydse koppelling. Daarna word die *Aktiewe Ruistal* en die *Aktiewe Ruistemperatuur* bereken. Hierdie nuwe parameters word bekendgestel om die gevolge van wedersydse koppelling op die ruisgedrag van die stelsel as 'n geheel te visualiseer.

Omdat FPA's per definisie groot is, vereis die analise daarvan deur middel van konvensionele metodes baie rekenaar hulpbronne. Hierdie metodes vereis dus die gebruik van rekenaarbondels of superrekenaars selfs gedurende die ontwerpfase van die antenna, wat baie duur en onprakties is. Daar is dus 'n metode ontwikkel wat gebruik maak van periodiese randvoorwaardes om groot antennaskikkings te analiseer. Die metode benader 'n groot antennaskikking as 'n eindig-opgewekte oneindige skikking van antennas. As gevolg hiervan, word die geheueverbruik met ordegroottes verbeter. Hierdie verbetering plaas dus die analise van groot antennaskikkings binne die vermoëns van huidige

persoonlike rekenaars. Die resultate wys ook 'n aanvaarbare graad van akkuraatheid vir gebruik gedurende die ontwerpfase van die skikking.

Die bykomende ruisdrwying op elke element as gevolg van wedersydse koppelling is ook bereken. Om dit te vermag, is daar 'n ekwivalente stroombaandiagram ontwikkel wat die gekoppelde stelsel in terme van die ruis- en transmissieparameters van die laeruisversterker (LNA) aan elke ontvangerkanaal en die koppelterme van die antenna skikking voorstel. Laastens word die aktiewe ruistal en die aktiewe ruistermperatuur ook bereken. Die teorie is geïmplimenteer deur gebruik te maak van 'n grafiesegebruikerskoppelvlak (GUI). Die GUI verskaf aan die gebruiker maklike toegang tot die teorie wat onwikkel is in hierdie navorsing. Daar is ook 'n snelnaslaantabel geskep met benaderde waardes van ruiskoppelling vir 'n verskeidenheid waardes van LNA ruistemperature en eerste element koppelling.

Die resultate van 'n 8×8 Vivaldiskikking voorbeeld, het 'n beduidende hoeveelheid ruiskoppelling getoon. Die ruiskoppelling het 'n maksimum toename in stelsel ruistemperatuur, T_{sys}, van ongeveer 9% van die LNA ruistemperatuur tot gevolg gehad. Volgens die huidige T_{sys} begroting van die SKA, kom dit neer op 'n T_{sys} toename van byna 1.3 Kelvin. In die konteks van die radioastronomie, kan hierdie toename in ruistemperatuur nie geïgnoreer word nie aangesien dit die bruikbaarheid van die teleskoop vir sekere velde van navorsing nadelig kan beïnvloed.

Acknowledgements

I would like to thank the following people for their support during the completion of this thesis.

- My Almighty Father: For giving me strength, perseverance and patience and everything else I needed to complete my thesis.
- My study leader, Professor K.D. Palmer: For your invaluable support. Thank you for sharing your knowledge with me.
- My fiancé, John: For his love and understanding. Thank you for your never-ending support.
- My parents: Thank you for always believing in me and for your constant encouragement.
- My brother-in-law, Eben: For your valuable last-minute insets.

Dedications

This thesis is dedicated to my parents, Derick and Annelie van der Merwe.

Contents

List of Figures

List of Tables

Nomenclature

Constants

$\pi =$	3.141 592 654
e =	2.718 281 828

Vectors and Tensors

$\overrightarrow{\boldsymbol{v}}$	Vector

Subscripts

a	Adiabatic
a	Coordinate

Abbreviations

EMI	Electromagnetic Interference
FDTD	Finite-difference Time-domain
FEM	Finite Element Method
FoV	Field of View
FPA	Focal Plane Array
GUI	Graphical User Interface
LNA	Low Noise Amplifier
MoM	Method of Moments
PAF	Phased Array Feed
RFI	Radio Frequency Interference
SKA	Square Kilometre Array
SNR	Signal-to-Noise Ratio

VLBI Very Long Baseline Interferometry

Chapter 1

Introduction

1.1 Radio Astronomy

As the term suggests, radio astronomy is a study of celestial bodies that emit radio waves. As the discovery of radio astronomy was dependant on advancements in radio engineering, which only started to flourish during the 1920's [1], radio astronomy is one of the younger branches of astronomy.

The emission of radio waves by celestial bodies had been theorised some time before its discovery in the early 1930's. In the 1860's, Maxwell's equations had shown electromagnetic radiation from stellar sources could exist at any wave-length [2].

In the early 1930's, the first identified radio source was discovered serendipitously. Karl Jansky, an engineer working for Bell Telephone Laboratories, was assigned to do research on sources of noise that interfered with short wave transatlantic voice transmissions. Using a large directional antenna, he noticed that his system kept recording a repetitive signal, the origin of which he could not trace. He also noticed that the signal peaked almost every 24 hours. Jansky concluded that the source of the radio-disturbance had to be associated with sources beyond the earth's atmosphere. As he continued his research, he showed that the sources of radiation were distributed throughout the Milky Way.

By the time Jansky concluded his work, another engineer named Grote Reber, started constructing a 9 m paraboloidal dish in his back yard in Wheaton, Illinois. At first, Reber could not duplicate the results obtained by Jansky due to limits in his equipment. However, after gradually adjusting to lower frequen-

cies, he finally succeeded in 1940. His results at 160 MHz were first published during the same year in the *Astrophysical Journal*. In 1944 Reber published another paper, which contained a detailed map of the radio sky. The two papers published by Reber caught the attention of astronomers world-wide. In the Netherlands, the director of Leiden Observatory, Jan Oort, brought Reber's 1940 paper to the attention of one of his colleagues, H.C van de Hulst, who then lead a discussion on it despite the war-time difficulties caused by German occupation. Within days, Van de Hulst showed that atomic hydrogen, which is the most abundant constituent of interstellar gas, should have a measurable spectral line at a wavelength of 21 cm. After the war, the Leiden Observatory was one of the first established radio observatories. In the next decade they established a major presence among other leading centres pursuing the new science of Radio Astronomy [3] [4].

In the years that followed, the science of Radio Astronomy has grown into an influential field of study. Of the ten astronomers who have won the Nobel Prize in Physics, six of them were radio astronomers.

Apart from being a major contributor to science during the last century, radio astronomy has proved to be the source of some major engineering endeavours. As the demand for larger reflectors, and better receiver systems grew, the challenges posed to the engineers assigned with designing and building it, grew as well. The result is that radio astronomers have a wide range of different techniques available to them in order to help them make observations. Radio Telescopes are the basic instruments used by radio astronomers and are discussed in detail in Chapter 2.

Achieving high resolution using only a single radio telescope proved to be difficult, which led to the development of radio interferometry. In radio interferometry, the signals from two or more radio telescopes are combined to improve the resolution. Effectively, an interferometer produces a beam with small dimensions which are dependent upon the observed wavelength and the baseline. The term *baseline* refers to the distance between the antennas. The resolution increases progressively as the baseline is increased. In order to achieve the longest possible baseline, astronomers record signals simultaneously at widely spaced telescopes. Observatories from all corners of the world participate in interferometry networks, known as Very Long Baseline Interferometry (VLBI) networks.

1.2 The Square Kilometre Array

Over the past several years, in several countries, discussions have been occurring about the next logical step in radio astronomy following the completion of the Atacama Large Millimetre/Sub-millimetre Array (ALMA). Development of a telescope providing two orders of magnitude increase in sensitivity over existing facilities at metre to centimetre wavelengths has been proposed. To realise this goal, a telescope with one square kilometre of collecting area is required. This is one hundred times larger than the collecting area of the Very Large Array (VLA) [5]. This initiative is called the Square Kilometre Array (SKA).

After extensive discussion of the technical possibilities and the science drivers, a concept for the SKA and a set of design goals have been created. The SKA will be an interferometric array of individual antenna stations, synthesizing an aperture with diameter of up to several thousand kilometres [5]. This will result in an extremely high angular resolution.

The SKA is aimed to have a large field-of-view (FoV). The goal is a FoV at frequencies of 200 square degrees below 1 GHz, and one of more than 1 square degree at higher frequencies. One exciting new development being explored is the use of Focal Plane Arrays (FPA's) to provide a multi-pixel capability that will further increase the FoV. The larger FoV could result in a dramatic increase in the survey speed of the SKA. Along with the possibility of achieving a large sky coverage with multiple FoV's, a major challenge in signal processing and computing is presented. More information on FPA's is given in Chapter 2.

As the SKA will be about 50 to 100 times more sensitive than any other radio telescope on Earth, it will be able to probe the edges of our Universe. This will enable scientists to answer fundamental questions in astronomy, cosmology and physics. The radio astronomy community has compiled a list of five key science drivers for the SKA. These key science drivers are [6]:

(a) The cradle of life,

(b) Probing the Dark Ages,

(c) The origin an evolution of Cosmic Magnetism,

(d) Strong field tests of gravity using pulsars and black holes, and

(e) Galaxy evolution, cosmology and dark energy.

Currently, South Africa and Australia have been short-listed as candidates to host the SKA. As a result, both countries are leading SKA Pathfinder projects, which are tasked with developing and building prototype systems which will be used to determine the key technologies for the SKA. South Africa's SKA Pathfinder is called the Karoo Array Telescope (MeerKAT). Even though MeerKAT is only a precursor to the SKA, it is considered to be amongst the largest and most powerful telescopes in the world.

MeerKAT is currently being constructed on a site adjacent to that of the proposed site for the SKA near the small town of Carnarvon in the Northern Cape Province. When finished, it will consist of 80 dishes with a high-speed data network linking the telescope site in the Karoo to the control centre in Cape Town. During the MeerKAT project, technologies appropriate to the SKA will be developed. These include composite, one-piece reflectors, single-pixel wideband receivers, low-cost, high-reliability cryogenic systems, and re-configurable digital processing systems. The telescope will be commissioned in 2013 [7].

The final site selection for the SKA will have been done by 2012, after which construction of the first phase at low and mid-frequencies will commence. The full telescope for observations at low and mid-frequencies will be completed between 2018 and 2022 [5].

1.3 Key Concepts

In this section, some key concepts that hold reference to the rest of this document are defined.

The following terms are associated with antenna arrays:

- *Antenna*. Refers to a single antenna in an array environment, without receiver circuitry.
- *Element*. Refers to a single antenna in an array environment, along with its receiver channel.

The following terms are associated with antenna modelling packages:

- *CST*. This an abbreviation used for CST Microwave Studio.

- *FEKO*. This refers to FEKO, which implies either CADFEKO, EDITFEKO or POSTFEKO, unless otherwise specified.

1.4 Outline of research

The research recorded in this document is done in chronological order, the goal being to investigate the effect mutual coupling has on the noise performance of Focal Plane Arrays. In order to do so, the problem at hand needs to be properly understood and defined.

In the theoretical framework and literature study (Chapter 2), background knowledge on radio telescopes in general are given. This is followed by factors contributing to noise in the radio signals received by the telescope. Next, background knowledge on Focal Plane Arrays are given, which is then followed by an introduction to noise coupling. In the last section, Floquet Theory for Infinite Arrays is introduced as infinite array analysis forms a significant part of the next chapter.

As noise coupling is a direct result of mutual coupling, it is necessary to calculate the mutual coupling terms first. In Chapter 3, a method is introduced that can be used to estimate the coupling terms of large arrays.

In Chapter 4, the noise coupling is calculated. This is done by developing an equivalent circuit model to represent the array of coupled elements. The terms *Active Noise Temperature* and *Active Noise Figure* are also introduced and derived.

In Chapter 5, the theory discussed in Chapters 2 to 4 are implemented using a Graphical User Interface (GUI) developed with MATLAB. The input required by the GUI is examined as well as the basic functioning of the script. The method of calculating the noise coupling as described in Chapter 4 is verified by means of an example. An example calculation of the noise coupling in an 8×8 element Vivaldi array is also performed and discussed in the context of the SKA.

Chapter 6 concludes and some recommendations are made for future projects.

Chapter 2

Theoretical Framework and Literature Study

2.1 Introduction

In this Chapter a theoretical framework and background knowledge relevant to the topic of this thesis are given. One aim of this chapter is to provide the reader with an insight into the functionality of a radio telescope, with a special focus on the instrumental requirements of the radio astronomer.

In Section 2.2 basic concepts relating to Radio Astronomy and Radio Telescopes are discussed. Section 2.3 gives an overview of noise in Radio Telescopes. Factors influencing the sensitivity of the telescope are discussed with special attention given to receiver noise. In Section 2.4 Focal Plane Arrays (FPA's) are discussed. What Focal Plane Arrays are, how they work, how they compare to the more traditional cluster of horn-antennas, and example elements currently being researched for their feasibility as focal plane array elements are examined. In Section 2.5 literature on noise coupling is reviewed. The importance of noise coupling, a method used to calculate the noise coupling and measurements of noise coupling in an FPA is discussed. In Section 2.6 an overview on infinite array analysis is given incorporating an introduction to Floquet Series Expansion and Floquet Modes. Section 2.7 summarises.

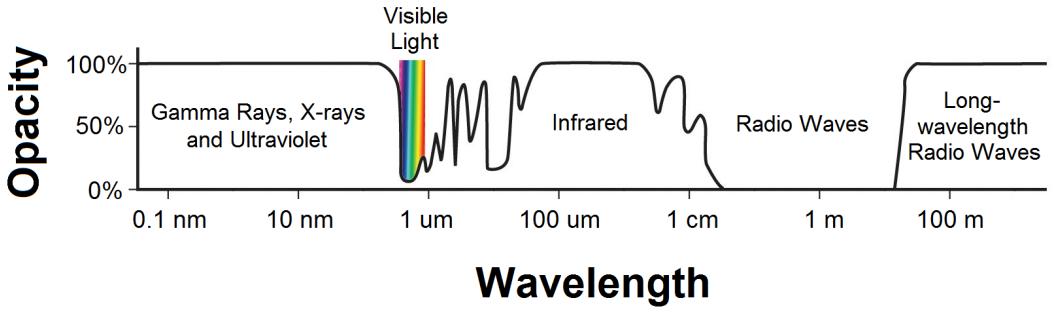

Figure 2.1: The Electromagnetic Spectrum (Credit: NASA/IPAC)

2.2 Radio Telescopes

This section discusses the basic concepts related to radio astronomy and radio telescopes. Where Radio fits into the wide field of astronomy, what observations are made using radio telescopes and the basic functionality of a radio telescope and its receiver system are reviewed [8]-[13].

A radio telescope is a type of telescope used by radio astronomers to make observations in the radio frequency portion of the electromagnetic spectrum. In essence, it is a type of directional antenna that detects and collects data from sources in the sky that emit electromagnetic waves. Usually radio telescopes are located far from cities and other sources of radio frequency interference (RFI), or electromagnetic interference (EMI).

Figure 2.1 illustrates the electromagnetic spectrum with regard to astronomical observability. It can be seen that radio astronomy fits roughly in the band between 1 centimetre and 1 kilometre wavelength. This is known as the Radio Frequency (RF) band. The opacity refers to the atmospheric opacity, which describes the reflection, absorption and scattering of waves entering the earth's atmosphere. Gamma rays, X-rays and ultraviolet light are completely blocked by the upper atmosphere, which means it is best observed from space. Visible light has some atmospheric distortion but is mostly observable from earth. Most of the infrared spectrum is absorbed by atmospheric gasses and is also more effectively observed from space. Radio waves are observable from earth but long-wavelength radio waves are blocked, which is why radio astronomy utilises both ground-based telescopes and space-telescopes.

Several objects in the Universe can only be studied using radio telescopes. Black Body Radiation from hot or warm objects such as the Cosmic Microwave

Background, the Sun and the planets. These are known as continuous sources of radiation and the relation between the intensity and the wavelength can be described by Planck's law in the same way as is done in Optical Astronomy. Another phenomena studied in radio astronomy, is Line Radiation from transitions within atoms or molecules. Line radiation typically comes from clouds of gas in space and can be detected in both emission and absorption. Synchrotron Radiation is radiation emitted from charged particles moving at speeds close to the speed of light (ultrarelativistic speeds) in magnetic fields. The reception of this type of radiation uncovered previously undetected Universe through the synchrotron emission of high-energy particles in stars, galaxies and quasars. At much longer wave-lengths, a broad range of phenomena are studied. These include thermal radiation from the 21 cm line of neutral Hydrogen found in a wide range of molecular lines that come from dense, cold gas concentrations that can be found within the interstellar medium.

The task of the radio astronomer is therefore to deduce the conditions under which the radiation received from the sky was emitted. In some cases they also determine the temperatures, compositions and distances of the radio sources and map the size and distribution of brightness for extended sources.

The functionality of a radio telescope closely resembles that of an optical telescope, even though it is not clear at first glance. The parabolic dish, used as a reflector, focuses the beams to the receiver in much the same way as the lenses in an optical telescope does. However, there is an obvious feature that sets a radio telescope apart from an optical one. The energy received by the instrument is not measured directly upon reception. Instead, the signal is processed and amplified before it is measured. This is done carefully to ensure that its wave-like character is preserved. The measurements represent the Universe in terms of intensity and state of polarisation as a function of time, frequency and angular position.

Figure 2.2 is a basic block diagram of telescope receiver system. The components consist of the antenna, a low noise amplifier (LNA), a receiver, a detector and finally a computer. In practice, the LNA is part of the receiver but because of the importance of the LNA in this project, it is illustrated as a separate part.

The signal, along with a considerable amount of noise, is received by the antenna and immediately amplified by the LNA. Usually, the whole receiver

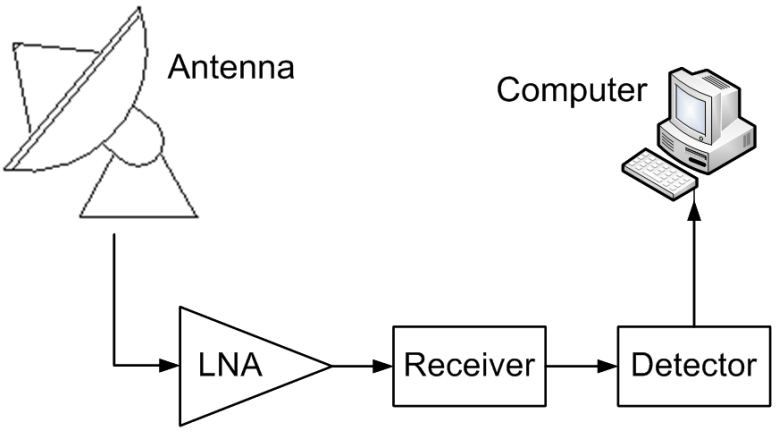

Figure 2.2: Radio telescope receiver diagram

system, including the antenna is cryogenically cooled to avoid additional thermal noise being added to the signal by the equipment. The detector is used to convert the amplitude output by the receiver, which is a voltage, to a power signal. This is simply done by multiplying the signal with itself, which is why the detector is sometimes called a *square-law device*. After the signal has been converted to a signal representing power, the signal still contains a great deal of noise. In other words, the signal is fluctuating. To rectify these fluctuations, a time-average of the signal is calculated, usually by means of an integrator. The output of the detector is then recorded by the computer.

In the next section, the receiver system is discussed in more detail, with particular attention given to noise and other factors limiting the sensitivity of the radio telescope.

2.3 Noise in Radio Telescopes

The level of research that can be done by astronomers is almost entirely determined by the quality of their instrumentation. Limitations of their equipment are the source of most of their frustration, which is why it is important for engineers to understand what the instrumental goals of astronomers are. The most important instrumental goals include greater angular resolution, obtaining a larger collecting area and more sensitive detectors.

2.3.1 Sensitivity of Radio Telescopes

The sensitivity of a radio telescope is defined as *a measure of the weakest source of radio emission that can be detected and is, therefore, directly related to the errors of measurement* [14]. The errors of measurement and limits of detection are affected by noise in the receiver voltage. Everything the signal comes into contact with can potentially add noise to it. As a result, the noise fluctuations of the signal are attributed to:

(a) *The signal itself.* All forms of radiation studied in radio-astronomy are governed by statistical laws. The measured power fluctuates around a mean value. To precisely measure the mean value, it is necessary to average the signal over a long time - in theory, an infinite period. This, of course, is not practical. As a result, measurements are merely averaged over seconds or minutes, which subsequently still leaves some percentage of noise in the signal.

(b) *The medium between the radio source and the telescope.* Scintillation may be produced due to clouds of gas in the interplanetary space. The earth's atmosphere, however, is of much greater concern. At long wave-lengths, variations in the earth's ionosphere affect the quality of the signal significantly, and at short wave-lengths, attenuation and scattering in the lower atmosphere is also troublesome.

(c) *Antenna characteristics.* The antenna characteristics are important for understandable reasons. Spillover can introduce unnecessary ground noise into the system, a poorly matched antenna will result in a portion of an already weak signal not to reach the receiver, etc.

(d) *Unwanted signals that reach the telescope.* These signals are typically from sources located in the side-lobes of the antenna or from thermal ground radiation. RFI is also a problem but more often than not, it can be recognised and corrected. Radio-telescopes are also placed in remote areas to make use of the curvature of the earth and natural barriers such as mountains in an attempt to block out RFI.

(e) *Receiver noise.* The signals received at medium and short wavelengths are so weak that additional receiver noise can drown out the signal completely.

At longer wavelengths, however, the sky is bright enough that the added receiver noise will not be such a major problem to any further extent.

(f) *Instabilities in the equipment.* Variations in equipment parameters can result in a false detection. Requirements in terms of stability are therefore very strict.

(g) *Time spent on a single observation.* Designing the telescope more carefully might reduce the time needed for any single observation, which suggests that more observations can be made.

(h) *The image forming characteristic.* The number of pieces of information produced simultaneously is also determined by the sensitivity of the telescope.

(i) *The size of the region of the sky that can be observed.* A larger field of view is a important key science issue for future radio telescopes [6].

2.3.2 Receiver Noise

As explained above, the noise the receiver adds to the system can significantly affect the sensitivity of the telescope. More exact knowledge about the receiver noise can therefore only be advantageous, since only a little extra noise from an unanticipated source can greatly reduce the usefulness of the telescope for certain areas of research.

Figure 2.3 is a block diagram representation of a typical heterodyne receiver system used in most radio-telescopes. In essence, it is a cascaded system of components, each component adding some noise to the signal. The type of noise added, is known as *thermal noise*, and is the most prevalent type of noise found in RF and microwave systems. Thermal noise is caused by the random motion of thermally excited carriers and is generated in any passive circuit element that contains loss, such as resistors, lossy transmission lines, and other lossy components.

In a cascaded system, such as the heterodyne receiver in Figure 2.3, each component will progressively degrade the signal-to-noise ratio (SNR). To evaluate the overall performance of the receiver, quantification of this degradation effect is done. Each component has a gain, G, and a noise temperature, T, both of which are used to calculate the overall noise temperature, T_{sys}, of the

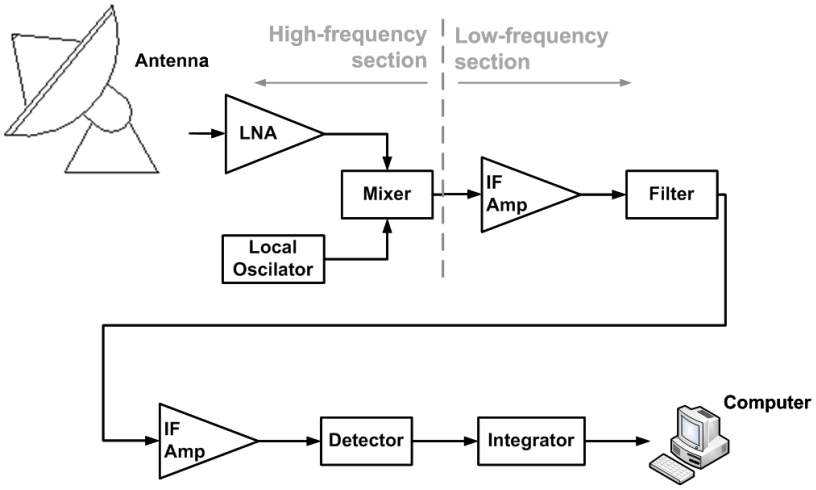

Figure 2.3: Block diagram of a basic heterodyne receiver.

system. The noise temperature of the cascaded system is therefore calculated as follows:

$$T_{sys} = T_1 + \frac{T_2}{G_1} + \frac{T_3}{G_1 G_2} + ... + \frac{T_N}{G_1 ... G_{N-1}}, \tag{2.3.1}$$

where T_N and G_N depicts the noise temperature and gain of the Nth element of the system.

It is clear from equation (2.3.1), that the noise temperature and gain of the first element in the system have the greatest effect on the overall noise temperature. The first element is therefore usually a special amplifier with exceptionally low noise, known as a *Low Noise Amplifier* (LNA). Even though the LNA is designed to add little noise to the signal, some noise is still added. The noise generated by the LNA is not only sent towards the receiver, but also back towards the antenna and radiated. When a single antenna, or an array of antennas with low mutual coupling is being used, the radiated noise originating from the LNA does not pose any problems, as it is not added to the signal. In more tightly coupled arrays, the noise couples to the other elements and increase the total system noise temperature, which in turn reduces the efficiency of the telescope. This phenomena is discussed in more detail in Section 2.5 and in Chapter 4.

In the next section, phased array feed systems, more commonly known as *Focal Plane Arrays*, are introduced.

2.4 Focal Plane Arrays

In this section, Focal Plane Arrays (FPA's) are discussed. What Focal Plane Arrays are, how they work, how they compare to the more traditional cluster of horn-antennas, and some example elements currently being researched for their feasibility as FPA elements are examined [15]-[23].

Some of the science goals of the SKA require a large field-of-view (FoV) [6]. In order to achieve such a large FoV, a multi-pixel array of antennas is placed in the focal plane of the reflector. Traditionally, this array consisted of a cluster of horns, which has been thoroughly researched and optimised, and the risks and shortcomings involved are widely understood. Recent technology developments in particularly data processing, however, has enabled the use of large, dense phased arrays as feeding elements for radio telescopes. These phased array feeding elements are known as Focal Plane Arrays (FPA's). It makes use of phased array technology, which, in theory, will enable the collection and manipulation of the entire electric field in the focal plane. This will in turn create the possibility of generating multiple beams while, at the same time, improving the illumination of the dish. As a result, the focal plane concept will give instruments a "multi-pixel" capacity similar to that of optical telescopes, which will, in effect, turn each telescope into a "radio-camera".

Implementation of multiple beam theory will require a prudent beam-former design. Beam-forming can be done in a number of ways, for example:

(a) *In the RF domain.* This method will make use of power combiners, analogue phase-shifters and amplitude control, which greatly simplifies prototyping. It is also the simplest method to use when upgrading existing feed-systems. Larger dishes used for wide-band operation at higher frequencies using a limited number of beams are a typical application for this method of beam-forming.

(b) *In the digital domain.* Here, different weights can be applied to the amplitude and phase of the signals using digital multiplication. This will require digitisation of each antenna signal, resulting in high volumes of data that need processing, which will increase the cost of the receiver system. Digital beam-forming can be done at the front-end but dealing with self-generated noise, size and power consumption will pose some other challenges. This method will typically be used when a large number of beams are required,

for instance in VLBI (Very Long Baseline Interferometry), where one beam can be used for calibrating the VLBI observation.

(c) *A combination of digital and analogue,* which utilises the best of both the digital and analogue worlds.

2.4.1 Strengths of FPA's

Figure 2.4: The horn cluster of the Parkes Multibeam Receiver [19]

FPA's differ from horn-clusters in that the antenna beam is composed using many antenna elements. To each element, a specific weight in phase and amplitude is given before the signals are summed. In a horn-cluster, each element represents one beam, which results in separate focal spots being sampled. The distances between the spots are determined by how closely the horns can be packed. Since the diameter of the horn is typically greater than the half-power diameter of the focal spot, the beams in the sky are spaced further apart than required by Nyquist sampling theory [24]. The result of this shortcoming is that the sky cannot be fully sampled. The situation is worse for wide-band feeds where the spacing between the elements is constant,

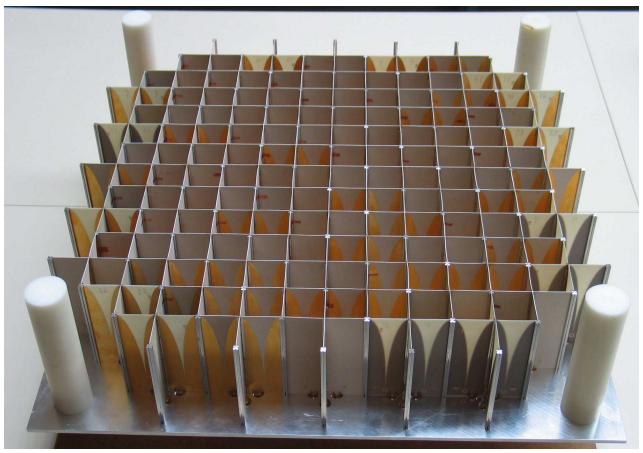

Figure 2.5: A prototype Vivaldi array [20]

while the beam-width and frequency are inversely proportional. The result is that the beam-widths at the high-end of the operating band are small, which implies that more observation time is required to create a fully sampled map of the sky. Figure 2.4 is the horn array used on the 21-cm Multibeam Receiver at Parkes Radio Observatory in Australia.

When using an FPA, an arbitrary number of beams can be formed and steered, which will enable adequate sampling of the sky, increasing the FoV [17], [22]. The increased FoV will in turn reduce observation time. The use of electronically synthesised multiple beams will also improve bandwidth, as the FPA feed characteristic can be changed to accommodate different frequencies and changes in the RFI environment. Compensation for polarisation errors and variations in the shape of the reflector due to gravity can also be done, as well as suppression of near-field scattering caused by the feed struts.

2.4.2 Weaknesses of FPA's

While the FPA and associated electronic feeding system has many promising features, these features generate limitations at the same time. For every beam adjustment, antenna parameters such as gain and active impedance change, which necessitates re-calibration of the whole system.

Radio Telescope efficiency is expressed in terms of $\frac{A_{eff}}{T_{sys}}$, where A_{eff} is the effective receiving area, and T_{sys} is the system temperature of the telescope [21]. The effective area is influenced by both the geometry of the dish and the antenna efficiency, while the antenna efficiency is influenced by, among

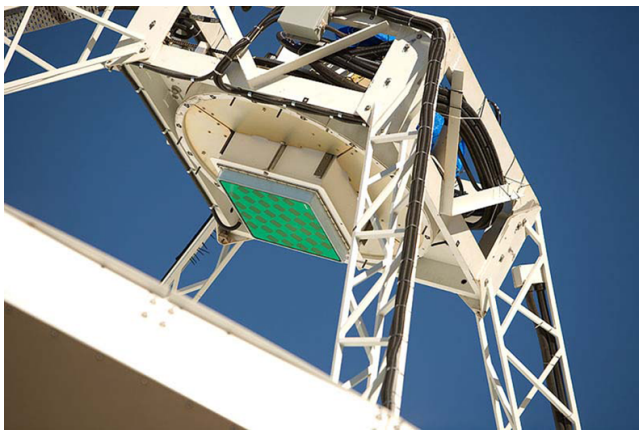

Figure 2.6: Prototype Checkerboard Array [23]

others, the blockage efficiency and the polarisation efficiency, both of which are slightly degraded by the FPA system.

In astronomy systems, cryogenic cooling is applied to achieve the low system temperature required in the 4-8GHz range [17]. The large number of Low Noise Amplifiers (LNA's) needed for FPA systems pose some challenges in the cryostat design with regard to power consumption and thermal leakage. When horn-antennas are used, the thermal leakage is addressed by placing the antennas into the cryostat as well, which reduces the amount of cables entering the cryostat. This method, however, requires careful design of the cryostat window in terms of losses and blockage. It has also proved technically difficult to cool large FPA's to cryogenic temperatures, which is why, to date, it has not been achieved yet.

2.4.3 Elements currently researched for FPA applications

In order for an antenna to be used as an FPA element, there are two main requirements: the possibility of close packaging, which requires the use of electrically small elements, and broad bandwidth [24].

Two possible candidate antennas have been identified and prototypes are currently being tested around the world.

(a) *Vivaldi element array.* In principle, Vivaldi antennas are capable of 7:1, or even 10:1 bandwidth. This makes the Vivaldi antenna attractive for use as an FPA element, even though the bandwidth is limited to ±3:1 in

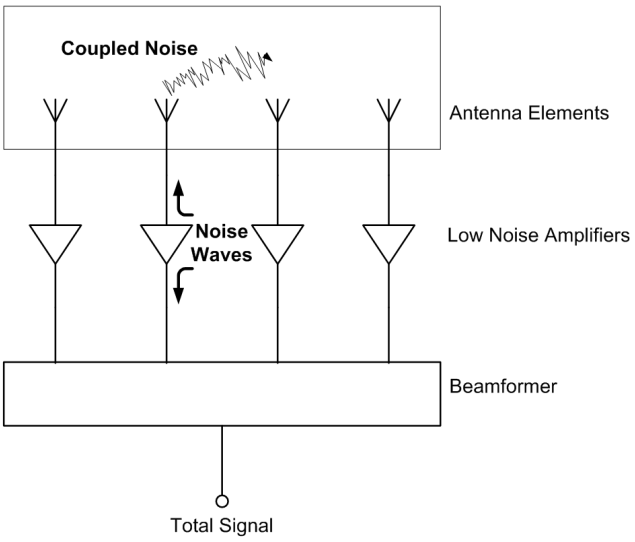

Figure 2.7: Illustration of the noise coupling in a Focal Plane Array

FPA application [17], [24]. An example of a prototype FPA consisting of Vivaldi elements can be seen in Figure 2.5.

(b) *The checkerboard array.* This FPA has been developed for AKSAP, the Australian SKA Pathfinder [16]. It is a dual-polarised connected "checkerboard" array. The complete structure consists of printed circuit board, foam and a ground-plane [23]. This design forms a robust and simple-to-manufacture structure. A prototype of the checkerboard array currently being tested at the 12-m Parkes Testbed Facility, can be seen in Figure 2.6.

2.5 Noise Coupling

Due to the tight packaging of antenna elements in FPA's, there is a high level of mutual coupling between the elements. The presence of mutual coupling between antenna elements is one of the features that set FPA's apart from horn fed reflector systems.

Noise generated by the LNA's connecting the antenna array to the receiver system, is not only sent towards the receiver, but also towards the antenna array. The mutual coupling between the antenna elements will result in noise power being coupled from one receiver channel to another, resulting in an

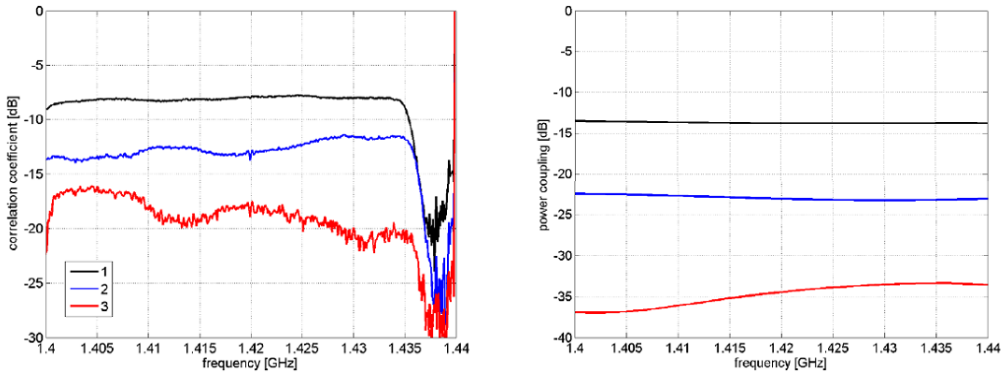

Figure 2.8: Measured cross-correlation between two antenna elements as function of their E-plane separation (left) and the measured mutual coupling coefficients between these elements measured in the laboratory (right) [22].

additional (correlated) noise contribution. This phenomena is known as *Noise Coupling* [22] and is described schematically in Figure 2.7.

In a large phased array, the coupled noise received by the other elements is amplified. This significantly degrades the performance of the array. The total contribution of the coupled noise to the system temperature is therefore an important consideration in radio-telescopes, where the system temperature directly influences the efficiency of the telescope. However, since there are so many parameters influencing the mutual coupling in scanning arrays, calculating the noise coupling is not a simple matter.

Ivashina et al. [21], [24] and van Cappellen et al. [22] highlight the importance of analysing the noise coupling in FPA's. However, methods on how to calculate the noise coupling are not provided. Van Cappellen [22] measures the noise coupling of an FPA consisting of 112 Vivaldi elements in two polarisations: X and Y. In Figure 2.8 (left), the magnitude of 3 of the measured cross-correlations for different element-separations in the E-plane can be seen. The top curve is that of two neighbouring elements, which, as can be expected, is the highest. The correlation decreases as the element separation increases. The figure on the right is that of the power coupling between the same elements. Although the measured power coupling is -14 dB for the two neighbouring elements, the cross-correlation coefficient is typically -8 dB. This discrepancy is due to the additional noise coupled from other elements in the array.

Weem and Popović [18] have shown that because the relative phase between

array elements change as the array is scanned, the noise coupling coefficients are a function of scan angle. Furthermore, they have shown that noise coupling is proportional to the active reflection coefficient, $\Gamma(\theta, \phi)$. Since $\Gamma(\theta, \phi)$ is such an easily measurable quantity, the conclusion they have drawn has been useful.

2.6 Floquet Theory for Infinite Arrays

Bhattacharyya explains the importance of undertaking infinite array analysis in his book [25]. He motivates his rationale by arguing that elements in the central region of an electrically large array have similar active reflection coefficient characteristics as that of an element in an infinite array.

In chapter 3 of this document, it is proved that the performance of an infinite array with finite excitation can be determined accurately by utilizing the results of an infinite array. The results of an infinite array, obtained using period boundary conditions, are applied to predict the mutual coupling between elements in a finite array.

As stated previously, Focal Plane Arrays are by definition large and densely packed arrays. This results in a high level of mutual coupling, which, in turn, causes a significant amount of noise coupling.

It is shown in chapter 3 that the memory required to analyse a large finite array exceeds the capabilities of current desktop computers. Infinite array analysis is therefore a practical solution to the problem of analysing large phased arrays.

This section gives an introduction to Floquet Modes in Infinite Arrays starting from the basic Fourier Transform. Characteristics of Floquet Modes with regard to antenna radiation are also explored [25].

2.6.1 Fourier Analysis and Floquet Series Expansion

A periodic function with periodicity a, such as a current distribution on an infinite array, can be expressed as follows:

$$g(x) = \sum_{n=-\infty}^{\infty} f(x - na) \tag{2.6.1}$$

Since phased arrays, which have progressive phase-shifts, are used, a more accurate expression for the current distribution is

$$h(x) = \sum_{n=-\infty}^{\infty} f(x - na)e^{(-jn\phi)}, \tag{2.6.2}$$

where ϕ is the constant phase-shift between elements.

Now, the Fourier Transform of equation (2.6.2) is

$$H(k_x) = \frac{1}{2\pi} \sum_{n=-\infty}^{\infty} e^{-jn\phi} \int_{-\infty}^{\infty} f(x - na)e^{(jk_x x)}dx. \tag{2.6.3}$$

Substituting $x - na$ with x‘ yields

$$H(k_x) = F(k_x) \sum_{n=-\infty}^{\infty} e^{-jn(k_x a-\phi)}. \tag{2.6.4}$$

Furthermore, the following identity exists for infinite series:

$$\sum_{n=-\infty}^{\infty} e^{(jnk_x a)} = \frac{2\pi}{a} \sum_{n=-\infty}^{\infty} \delta(k_x - \frac{2n\pi}{a}). \tag{2.6.5}$$

Using the identity in equation (2.6.5), the Fourier transform becomes:

$$H(k_x) = \frac{2\pi}{a} F(k_x) \sum_{n=-\infty}^{\infty} \delta\left(k_x - \frac{2n\pi}{a} - \frac{\phi}{a}\right). \tag{2.6.6}$$

It can be seen that the spectrum exists at discrete intervals. The spectral lines, however, deviate from that of a periodic function without a progressive phase-shift by an amount $\frac{\phi}{a}$. This is illustrated in Figure (2.9) where (a) represents the spectra of a function without progressive phase-shift, and (b) the function with progressive phase-shift where the $\frac{\phi}{a}$ deviation can be seen.

Now, $h(x)$ is written in terms of a series of complex exponential terms, e.g.

$$h(x) = \frac{2\pi}{a} \sum_{n=-\infty}^{\infty} F\left(\frac{2n\pi + \phi}{a}\right) e^{\left(-j\left(\frac{2n\pi+\phi}{a}\right)x\right)}. \tag{2.6.7}$$

This is the Fourier Series Expansion of an infinite period source.

The expression in equation (2.6.7) is called the *Floquet Series Expansion.*

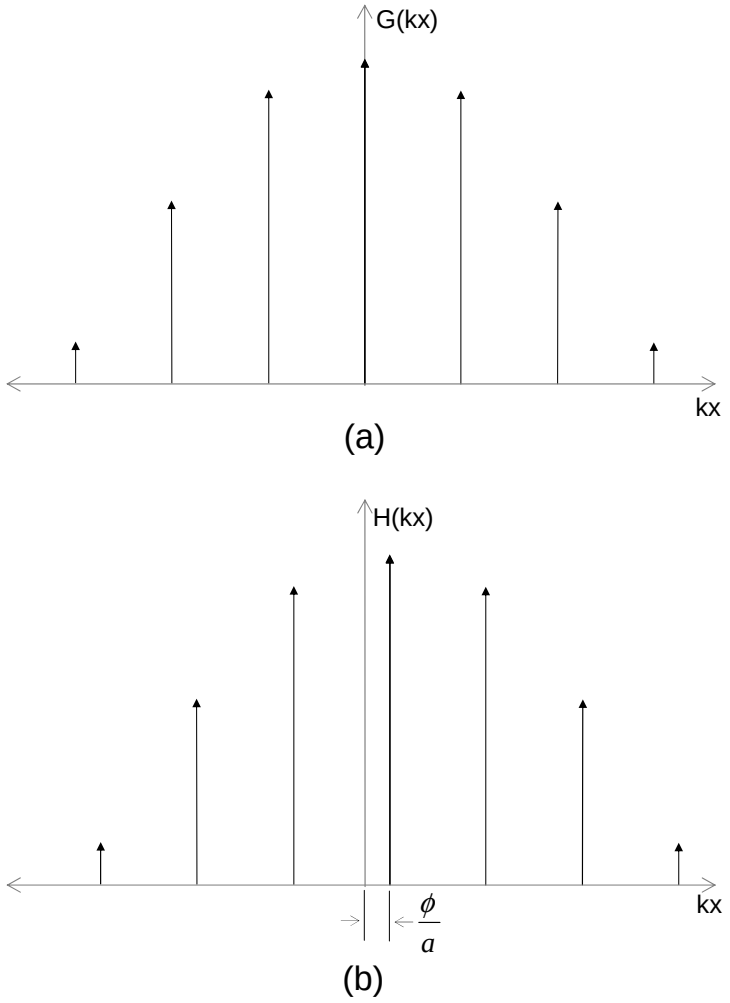

Figure 2.9: Discrete spectra of (a) g(x) and (b) h(x)

This is similar to the Fourier Series Expansion with the addition of the progressive phase-shift. This means, that if the progressive phase-shift should be zero, the function would resemble a normal Fourier Series.

Following the same procedure as above, for two dimensions, the two-dimensional Floquet Series Expansion is derived. This would be useful for planar arrays. Since there are many different grid structures for planar arrays, the form of the Floquet Series Expansion for every structure would differ.

2.6.2 Floquet excitations and the E-field

In the previous section the Floquet Series Expansion was introduced as given in equation (2.6.7). The electromagnetic fields produced by the array of current sources examined in the previous section are discussed in this section.

An array of current sources represented by equation (2.6.7)is called Floquet Sources because the fields they produce can be represented by Floquet Modal Functions as is explained below.

For the example that follows, the following assumptions are made:

- The sources are y-directed
- The sources are uniform along y
- The source current is a surface current located in the $z = 0$ plane

Making these assumptions insures that the problem is one dimensional.

The surface current excitation function is expressed as

$$\vec{I_y} = \sum_{n=-\infty}^{\infty} f(x - na)e^{(-jn\phi)}. \tag{2.6.8}$$

This will produce TM_y-fields that can be calculated using the vector potential, $\vec{A} = \hat{y}A_y$, that satisfies the Helmholz equation:

$$\nabla^2 A_y + k_0^2 A_y = -J_y, \tag{2.6.9}$$

where J_y represents the y-component of the volume current density. In this case, the height in the z-direction is infinitesimal small. This implies that the volume current density, $\vec{J_y}$, can be expressed in terms of the surface current

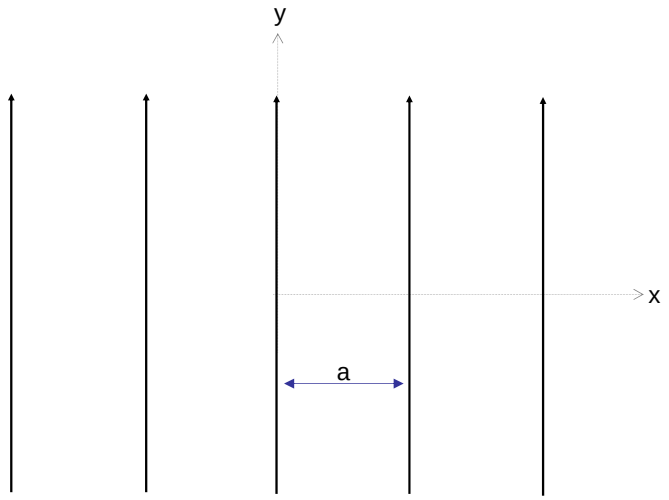

Figure 2.10: Linear infinite array of y-directed current elements

density, $\vec{I_y}$, multiplied by an impulse in the z-plane, $\delta(z)$, as follows:

$$\nabla^2 A_y + k_0^2 A_y = \delta(z) \sum_{n=-\infty}^{\infty} f(x - na) e^{(-jn\phi)}. \tag{2.6.10}$$

The surface current density can also be expressed as a Floquet Series which assists in finding a solution for A_y:

$$\nabla^2 A_y + k_0^2 A_y = \delta(z) \frac{2\pi}{a} \sum_{n=-\infty}^{\infty} F\left(\frac{2n\pi + \phi}{a}\right) e^{\left(-j\left(\frac{2n\pi+\phi}{a}\right)x\right)}. \tag{2.6.11}$$

Inspection of equation (2.6.11) yields the following possible solution for A_y:

$$A_y = \sum_{n=-\infty}^{\infty} F_n(z) e^{\left(-j\frac{2n\pi+\phi}{a}x\right)}. \tag{2.6.12}$$

Now a differential equation for $F_n(z)$ is formed by substituting equation (2.6.12) into equation (2.6.11) and comparing them term by term:

$$\frac{\partial^2 F_n(z)}{\partial^2} + k_{zn}^2 F_n(z) = -\delta(z) \frac{2\pi}{a} F(k_{xn}), \tag{2.6.13}$$

With:

$$k_{zn}^2 = k_0^2 - k_{zn}^2 \qquad k_{xn} = \frac{2n\pi + \phi}{a}. \tag{2.6.14}$$

One solution for $F_n(z)$ in equation (2.6.13) in free space, where $z > 0$ is:

$$F_n(z) = \frac{\pi}{jak_{zn}} F(k_{xn}) e^{(-jk_{zn}z)} \qquad . \tag{2.6.15}$$

This yields the following result for A_y:

$$A_y = \frac{\pi}{ja} \sum_{n=-\infty}^{\infty} \frac{F(k_{xn})}{k_{zn}} e^{(-jk_{xn}x - jk_{zn}z)} \qquad , z > 0. \tag{2.6.16}$$

Now, the electromagnetic field components are calculated using:

$$\vec{H} = \frac{1}{\mu} curl(A) \qquad \vec{E} = \frac{1}{j\omega\varepsilon_0} curl(\vec{H}). \tag{2.6.17}$$

From equation (2.6.17) it can be seen that $E_x = E_z = 0$, and $E_y = -j\omega A_y$, which means that the E-field radiated in the $z > 0$ direction is expressed in terms of an infinite series as

$$E_y = -\frac{\pi\omega}{a} \sum_{n=-\infty}^{\infty} \frac{F(k_{xn})}{k_{zn}} e^{(-jk_{xn}x - jk_{zn}z)} \qquad , z > 0. \tag{2.6.18}$$

In terms of antenna radiation, each exponential term inside the summation is called a Floquet Modal Function, or a Floquet Mode and satisfies the wave equation. Each Floquet Mode is thus associated with a plane wave propagating in a specific direction given by

$$\vec{p_n} = k_{xn}\vec{e_x} + k_{zn}\vec{e_z}. \tag{2.6.19}$$

The propagation vector associated with each Floquet mode makes an angle, θ_n, with the z-axis. This angle is given by:

$$tan\,(\theta_n) = \frac{k_{xn}}{k_{zn}} = \frac{k_{x0} + \frac{2n\pi}{a}}{\sqrt{k_0^2 - \left(k_{x0} + \frac{2n\pi}{a}\right)^2}}, \tag{2.6.20}$$

where $k_{x0} = \frac{\phi}{a}$. The dominant mode would be the Floquet mode corresponding to $n = 0$ since it propagates along the intended scan angle given by

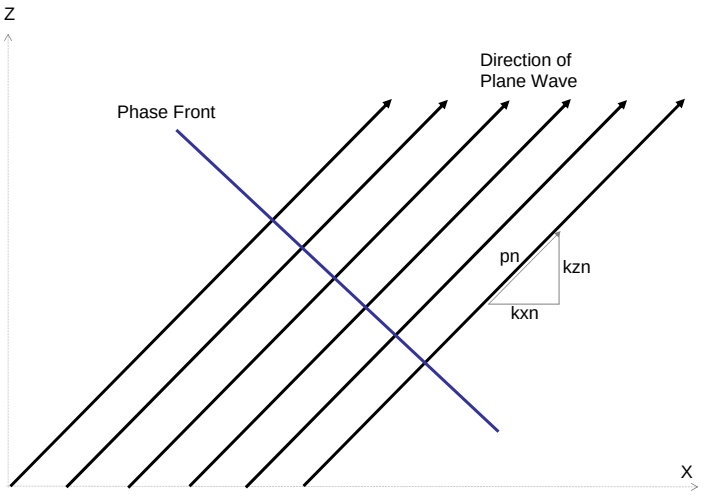

Figure 2.11: Direction of plane wave for one Floquet Mode

$\theta_0 = \arcsin\left(\frac{\phi}{a}\right)$. Other modes with real k_{zn} are considered grating beams. When k_{zn} is imaginary, the modal field components will decay with z, these are referred to as evanescent modes and will have an imaginary propagation angle θ_n. Typically, only a finite number of Floquet modes are propagating while the rest are evanescent.

2.7 Summary

In this chapter, background knowledge on radio telescopes was given with regard to the instrumental goals of the radio astronomer. Factors influencing the sensitivity of Radio Telescopes were therefore discussed with special focus on the receiver noise.

Focal Plane Arrays were introduced and compared to the more traditional cluster of horns. The strengths and weaknesses of FPA's were also highlighted and antenna elements currently investigated for their feasibility in FPA applications examined.

Next, an overview on Noise Coupling was given. Some previous studies that have been done on the subject were discussed.

The last section introduces Floquet Theory for Infinite Arrays. This forms a basis for the infinite array theory that is used in Chapter 3.

Chapter 3

Mutual Coupling

3.1 Introduction to Mutual Coupling and Scattering Parameters

This introductory section discusses the necessary background theory on Mutual Coupling and Scattering Parameters (S-parameters). Subsequently, the method of estimating the S-parameters for a finite array using results of an infinite array is discussed in detail, while presenting the results of an example calculation.

From Figure 3.1, it can be observed that antenna A is connected to an

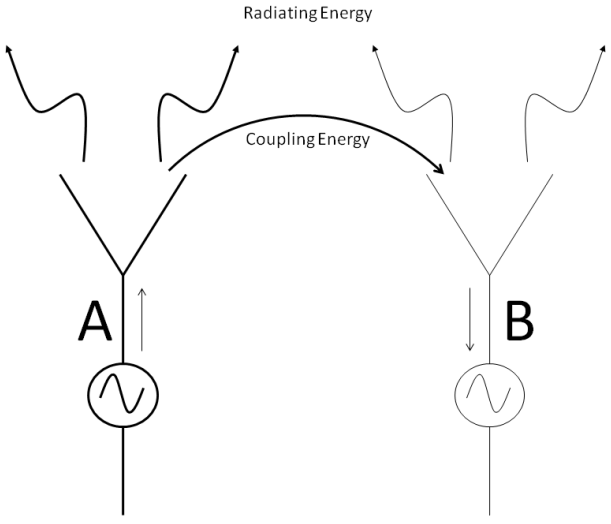

Figure 3.1: Mutual Coupling between antennas.

active source and antenna B to a passive one. This implies that antenna A produces an electromagnetic wave that propagates into free space. A fraction of the radiated energy is received by antenna B, inducing a current on the element. A part of the induced energy travels toward the passive generator on element B, and another part is reflected and re-radiated. Some of the re-scattered energy will be received by antenna A again, repeating the cycle.

From an observation point in space, the total energy would therefore not only come from element A, which is the excited element, but from element B as well.

When both elements are excited simultaneously, there is induced energy in both elements. Thus, the total contribution to the far-field pattern of a particular element in the array depends not only upon the excitation furnished by its own generator (in the direct excitation) but upon the parasitic excitation as well, which depends upon the coupling from and the excitation of the other generators [26].

It is important to know how much mutual coupling there are between array elements, because energy originating from element A, received by element B adds vectorially to the reflected energy from element B itself. This enhances the existing standing wave pattern on element B, which eventually changes the active port impedance for this element. This suggests that an isolated antenna might be well matched to the system it is attached to, but when positioned in an array environment it becomes mismatched. Mutual coupling therefore influences important array parameters such as:

- input impedance
- reflection coefficient
- passive element pattern
- active element pattern

The S-parameters are numerical values used to describe the mutual coupling between elements. They indicate what fraction of the energy applied to one element of an array, is received by another element in the array. This is shown in the following equation:

$$S_{mn} = \frac{V_m^-}{V_n^+}, \tag{3.1.1}$$

where:

- V_m^- is the voltage received at the port of antenna m,
- V_n^+ is the voltage applied at the port of antenna n.

Therefore, S_{mn} indicates how much of the energy applied to the port of antenna n, is received at the port of antenna m.

There are also other parameters that describe the mutual coupling between elements of an array, for example the Z-parameters, which measures the voltage induced on one element, due to a current on another, for example:

$$Z_{mn} = \frac{V_m}{I_n}. \tag{3.1.2}$$

The Y-parameters, which are the inverse of the Z-parameters are given by $([Y] = [Z]^{-1})$.

The remainder of the chapter summarises conventional methods used to calculate the coupling terms of an array. This is followed by the development and implementation of an alternative method that can be used to estimate the coupling terms of a finite phased array.

3.2 Summary of conventional methods used to calculate the coupling terms

Simulation packages such as FEKO [27] use the same principles to approximate the coupling terms of a system with multiple ports (e.g. an antenna array) as measuring equipment, like vector network analysers.

One port at a time is excited with a signal of specific frequency, amplitude and phase, while all the other ports are passive. The amplitude and phase of signals received by all the passive ports are then measured, and the coupling terms calculated using equation (3.1.1).

To achieve this computationally, the structure in question has to be characterised first. This is done by dividing the structure into a number of smaller elements in a process called meshing. Each mesh element is functionally dependant on all other mesh elements. This functional dependence is called a basis- (or expansion-) function. By solving all the basis-functions, the whole

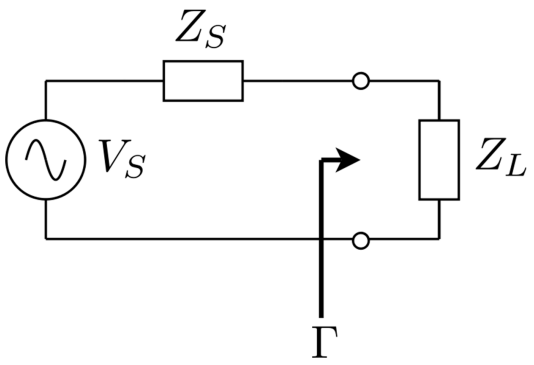

Figure 3.2: Sample Circuit cofiguration depicting the measurement location of the reflection coefficient.

structure can be characterised. The finer the structure is meshed, the more accurate the approximation to the real structure becomes, improving the accuracy of the result. This will, however, yield more basis functions to solve, requiring more memory and computation time [28].

The Method of Moments (MoM), which is a method used to characterise a structure by calculating the surface currents, treats each of N basis functions separately, which results in an N^2 scaling of memory requirements and N^3 scaling of calculation time needed to solve the set of equations [27].

In an antenna array with M identical elements, each described by N basis functions, the memory requirements are scaled by $(MN)^2$, which quickly exceeds the capabilities of desktop computers currently available. This makes it worthwhile to investigate other methods of estimating the coupling terms of an antenna array, which is what the remainder of this chapter is devoted to.

3.3 The Active Reflection Coefficient

The reflection coefficient is used when a wave propagating in a medium containing discontinuities is considered. In the case where an antenna is connected to a receiver circuit, the discontinuity is in the characteristic impedance of the various components of the circuit, and will occur at the connection point between the antenna and the receiver circuitry.

The law of maximum power transfer implies that the maximum amount of power will be transferred between a source and a load when the characteristic impedance of the source and the load are equal (matched) [29]. When the source and the load impedances are not matched and the maximum amount of

power is not transferred, the power not transferred to the load will be reflected back to the source. The amount of energy that is reflected back to the source is described by the reflection coefficient, which relates the incident signal with the reflected signal as follows:

$$\textit{reflection coefficient} = \frac{\textit{reflected signal}}{\textit{incident signal}},$$
$$\Gamma = \frac{V^-}{V^+}. \tag{3.3.1}$$

As reflection is a direct result of a mismatch between source and load impedance, the reflection coefficient can also be expressed in terms of the source and load impedances, denoted by Z_S and Z_L respectively and with reference to Figure 3.2, e.g.

$$\Gamma = \frac{Z_L - Z_S}{Z_L + Z_S}, \tag{3.3.2}$$

which shows that any variation in both the source- and load impedance will change the amount of energy reflected from the load.

The components of the circuit in Figure 3.2 can also represent an antenna connected to a receiver system as follows:

- V_S is the signal received by the antenna
- Z_S is the characteristic impedance of the antenna
- Z_L is the characteristic impedance of the receiver circuit

The characteristic impedance of an antenna is the impedance seen looking in at the port of the antenna. This impedance is therefore also known as the *input impedance*, which is a relation of the voltage and current received at the port,

$$Z_{in} = \frac{V_{in}}{I_{in}}, \tag{3.3.3}$$

and will therefore be influenced by all the voltages and currents induced on the antenna, including those currents and voltages that are induced due to mutual coupling. For instance, in a 3 antenna phased array with constant amplitude and progressive phase difference, α, the input impedance on the first element can be written as

$$Z_{in1} = Z_{11} + Z_{12}\frac{I_2}{I_1} + Z_{13}\frac{I_3}{I_1}, \tag{3.3.4}$$

with

- Z_{in1} the input impedance of the first element in an array environment
- Z_{11} the input impedance of an isolated antenna element
- Z_{12} and Z_{13} the impedance coupling terms.

As the amplitudes are constant in the current ratios of Equation (3.3.4) and the phase difference progressive, the resultant current ratios consists if only a phase term, e.g.:

$$Z_{in1} = Z_{11} + Z_{12}e^{j\alpha} + Z_{13}e^{j2\alpha}. \tag{3.3.5}$$

Equation (3.3.5) shows that the value of the progressive phase difference will have an impact on the value of the input impedance of an element in an array environment even though the mutual coupling terms remain constant.

The varying antenna input impedance when an antenna is placed within an array environment will result in the reflection coefficient varying with phase difference as well. The varying reflection coefficient is known as the *active reflection coefficient* [25].

3.4 Estimating the Coupling Terms of a Finite Phased Array by using the Characteristics of an Infinite One

As explained in Section 3.1, the S-parameters of an antenna array are numerical values that describe the amount of mutual coupling that occurs between the elements of an array.

In this section, a method is developed to estimate the coupling terms of an infinite phased array with finite excitation using theory related to one with infinite excitation. The rationale behind approaching the analysis of large phased arrays from this perspective, is to permit the use of the Periodic Boundary Condition (PBC) feature offered by both FEKO and CST. This feature analyses a single element in an infinite array environment. By employing this capability, it will greatly improve the memory usage as only the basis functions for a single element will need to be solved.

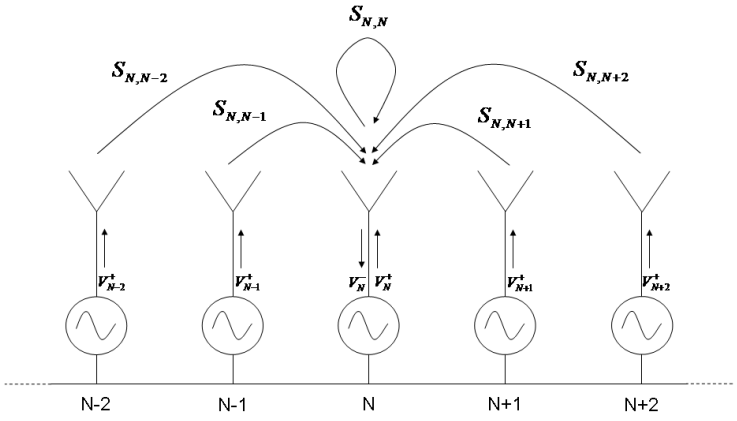

Figure 3.3: Coupling to the Nth element of an infinite phased array.

The active reflection coefficient of a single element (the Nth element) in an infinite array environment is:

$$\Gamma_N = \frac{V_N^-}{V_N^+}, \tag{3.4.1}$$

where

- V_N^+ is the applied signal, and
- V_N^- the incoming signal.

In an infinite phased array, the incoming signal of the Nth element can be described by the signal applied to each of the elements, as well as its coupling coefficient, as illustrated in Figure 3.4,e.g.

$$V_N^- = ...S_{N,N-1}V_{N-1}^+ + S_{N,N}V_N^+ + S_{N,N+1}V_{N+1}^+... \tag{3.4.2}$$

Now, dividing each term by the signal applied to the Nth element, V_N^+, results in an expression for the reflection coefficient of the Nth element:

$$\frac{V_N^-}{V_N^+} = ...S_{N,N-1}\frac{V_{N-1}^+}{V_N^+} + S_{N,N}\frac{V_N^+}{V_N^+} + S_{N,N+1}\frac{V_{N+1}^+}{V_N^+}... \tag{3.4.3}$$

The signal applied to the nth element of a phased array,

$$V_n^+ = V_0 e^{-jn\alpha}, \tag{3.4.4}$$

is a signal with a constant amplitude, V_0, and progressive phase, $n\alpha$.

Using equation (3.4.3) and (3.4.4), the following can thus be deduced:

$$\begin{aligned}\frac{V_N^-}{V_N^+} &= ...S_{N,N-1}\frac{V_0 e^{-j(N-1)\alpha}}{V_0 e^{-j(N)\alpha}} + S_{N,N}\frac{V_0 e^{-j(N)\alpha}}{V_0 e^{-j(N)\alpha}} + S_{N,N+1}\frac{V_0 e^{-j(N+1)\alpha}}{V_0 e^{-j(N)\alpha}}... \\ &= ...S_{N,N-1}e^{j\alpha} + S_{N,N} + S_{N,N+1}e^{-j\alpha}... \\ &= \sum_{n=-\infty}^{\infty} S_{N,n}e^{-jn\alpha}. \end{aligned} \tag{3.4.5}$$

Incorporating Equation (3.4.1), the active reflection coefficient is represented by

$$\Gamma_N(\alpha) = \sum_{n=-\infty}^{\infty} S_{N,n}e^{-jn\alpha}. \tag{3.4.6}$$

For an array of m elements, the S-parameters can be solved simultaneously for m different values of Γ, which can be obtained by using m different values for α. Thus, for an infinite array, an infinite number of values for α must be used. However, α is an angle with values $-\pi \leq \alpha \leq \pi$. It is also important to note that Equation (3.4.6) resembles a Fourier series, which enables the use of Fourier Theory to solve the coupling terms [30],e.g.:

$$S_{N,n} = \frac{1}{2\pi}\int_{-\pi}^{\pi} \Gamma_N(\alpha)e^{jn\alpha}d\alpha \tag{3.4.7}$$

This method can also be expanded to represent a two-dimensional rectangular array, e.g.:

$$S_{mn} = \frac{1}{4\pi^2}\int_{-\pi}^{\pi}\int_{-\pi}^{\pi} \Gamma_{00}\left(\alpha_x, \alpha_y\right) e^{j(m\alpha_x + n\alpha_y)}d\alpha_x d\alpha_y. \tag{3.4.8}$$

In this case, S_{mn} is an abbreviation for $S_{00,mn}$, where

- the subscript "00" indicates the central element of the array,
- m indicates how far the element from which the coupling is calculated, is removed from the central element along the x-axis, and

- n indicates how far the element from which the coupling is calculated, is removed from the central element along the y-axis.

The derivation above proves the possibility of solving the coupling terms of an array using a Fast Fourier Transform (FFT).

3.5 Z- and Y-parameters

The afore mentioned theory as per Section 3.4 can also be applied to calculate the impedance and admittance matrix from the active port impedance and admittance. Since it would be preferable to use this theory to calculate the parameters for FPA's, which are two-dimensional arrays, expressions for the impedance and admittance matrices of two-dimensional arrays are derived.

Starting with the definition of mutual impedance, the voltage of an element can be connected with the current excitation of all others as follows:

$$V_{00,active} = \sum_{m=-\infty}^{\infty} \sum_{n=-\infty}^{\infty} I_{mn} Z_{mn}. \tag{3.5.1}$$

Assume the amplitude of all the elements are uniform with progressive phase:

$$I_{mn} = I_{00} e^{-j(m\alpha_x + n\alpha_y)}. \tag{3.5.2}$$

The active input impedance seen by element (x, y)=$(0, 0)$ is therefore:

$$Z_{00}(\alpha_x, \alpha_y) = \frac{V_{00}}{I_{00}} = \sum_{m=-\infty}^{\infty} \sum_{n=-\infty}^{\infty} Z_{mn} e^{-j(m\alpha_x + n\alpha_y)} \tag{3.5.3}$$

As previously mentioned, this resembles a Fourier Series Expansion. Z_{mn} can therefore also be calculated using Fourier Theory:

$$Z_{mn} = \frac{1}{\pi^2} \int_0^{\pi} \int_0^{\pi} Z_{00}(\alpha_x, \alpha_y) e^{j(m\alpha_x + n\alpha_y)} d\alpha_x d\alpha_y. \tag{3.5.4}$$

To calculate the mutual admittance, a similar method, and the relationship $Y_{00} = \frac{1}{Z_{00}}$, is applied:

$$Y_{mn} = \frac{1}{\pi^2} \int_0^{\pi} \int_0^{\pi} Y_{00}(\alpha_x, \alpha_y) e^{j(m\alpha_x + n\alpha_y)} d\alpha_x d\alpha_y. \tag{3.5.5}$$

Equations (3.5.1) through (3.5.5) proves that, as would be expected, the same method as was used in Section 3.4 can be applied to calculate the impedance and admittance matrices of a phased array.

3.6 Symmetry

Consider Equation (3.4.8) again:

$$S_{mn} = \frac{1}{4\pi^2} \int_{-\pi}^{\pi} \int_{-\pi}^{\pi} \Gamma_{00}\left(\alpha_x, \alpha_y\right) e^{j(m\alpha_x + n\alpha_y)} d\alpha_x d\alpha_y. \tag{3.6.1}$$

The physical implication of this equation is that if the active reflection coefficient of a central element of an array can be calculated for a range of constantly increasing values of phase difference between $-180°$ to $180°$, the coupling terms can be calculated using an FFT. This can be achieved by using the periodic boundary condition functionality of an antenna modelling package. This will calculate the active reflection coefficient of an infinite phased array with linearly spaced elements.

It should be noted that the $-180°$ to $180°$ range of phase differences implies a $360°$ range of phase differences, with $0°$ phase difference resulting in a beam at bore-sight. For a linearly spaced array, the active reflection coefficient will be symmetrical around bore-sight in both dimensions. This means that all the information required is contained in only one half of the $\Gamma\left(\alpha\right)$ function per dimension, resulting in a reduction of calculation time by a factor of 2 for a one dimensional array, and a factor of 4 for a two dimensional one. A phase difference range of $0°$ to $180°$ instead of $-180°$ to $180°$ can thus be used per dimension.

3.7 Aliasing Considerations

In signal processing, aliasing refers to the signal distortion that occurs when an under-sampled signal is reconstructed to its original continuous form.

A signal is under-sampled when it is sampled at a frequency below its Nyquist frequency, which is defined to be $f_{Nyquist} = 2W$, where W is the maximum frequency component of the signal. To exactly reconstruct a signal

and therefore avoid aliasing, the sampling frequency has to be greater than the Nyquist Frequency [32].

Fourier theory is most commonly applied in the time-frequency domain. This time-frequency relationship is mirrored in this document by the $S(n) \Leftrightarrow \Gamma(\alpha)$ relationship. The analogue of the time domain is therefore the S-domain, and the analogue of the frequency-domain is the Γ-domain.

In the theory developed in the preceding sections, the function, $\Gamma(\alpha)$, continuous for $-\pi \leq \alpha \leq \pi, \alpha \in \Re$, is only calculated for discrete values of α, which is in effect a form of sampling. The function, however, is in the Fourier domain, which means sampling it will be similar to frequency domain sampling. The aliasing will therefore occur in the S-domain, which is a more complex problem to address. The continuous form of the S-function, which is not a practically realisable function but is considered from a purely mathematical point of view, is an infinite function which converges to zero in both positive and negative directions. Aliasing in the S-domain is therefore unavoidable.

However, there is a noise-floor in the S-domain below which accuracy is greatly reduced at any rate. The noise-floor is partly due to quantisation noise added to the calculation as a result of meshing. The most significant contributor to the noise-floor in this case, is the approximation noise. Since a large array is approximated by an infinite array, the estimation error will also contribute to the level of inaccuracy at the edges of the array.

Should aliasing occur below the noise-floor, the aliasing will not affect the usable data. The value of the noise-floor will vary with mesh-size, the geometry of the element and the number of elements in the array. It can therefore not be precisely determined prior to calculation.

Tests have shown that if four times the number samples of $\Gamma(\alpha)$ are taken than the desired number of elements in array, the effect of aliasing is completely covered by the noise-floor. This effect can be seen in Figure 3.4, where the effect of $2\times$, $4\times$ and $8\times$ the number of desired elements are taken for the FFT method, and then compared to the results obtained by a brute-force calculation. It can be seen that enlargements above $4\times$ did not produce any notable improvements in accuracy. The test above was repeated where the geometry of the test-elements were exceptionally finely meshed in an attempt to negate the effect of the quantisation noise. The same conclusions were drawn from those tests as from the test above. One can therefore assume that this

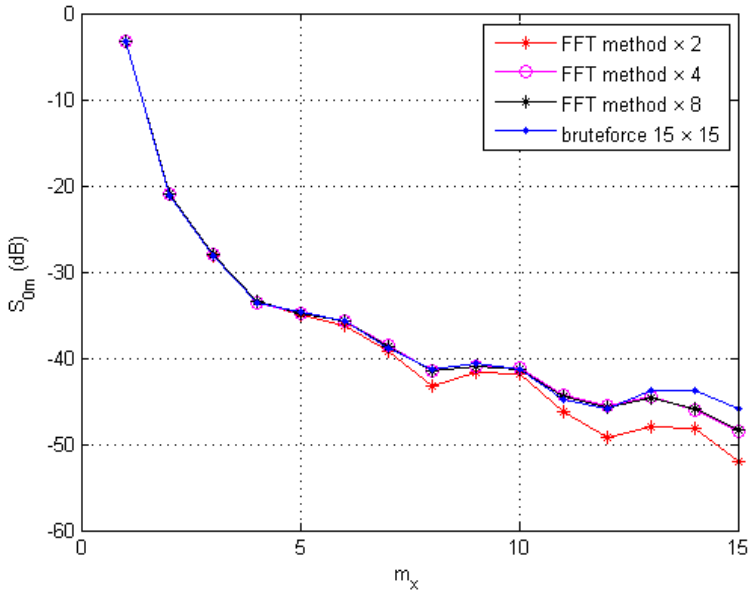

Figure 3.4: Anti-aliasing attempts

method of aliasing avoidance should still suffice when, under normal meshing circumstances, the quantisation noise becomes significant by lifting the noise floor to a higher level.

3.8 Memory usage

In Section 3.2, memory usage was given as the primary motivation for investigating an alternative method to calculate the coupling terms of a phased array. This Section is devoted to illustrating the improvement in memory requirements the FFT method (PBC-MoM) demonstrates in comparison with the brute-force MoM.

Figure 3.5 shows the memory usage for both the PBC-MoM, and the brute-force MoM methods. The example element used was a simple flat dipole with respectively 16 and 32 mesh-cells per element for a single frequency point.

The brute-force method will add another 16 or 32 mesh-cells to the calculation for each element added to the array. Since the memory requirements increase with a square-law [27], the brute-force calculation for even a simple structure like this quickly exceeds the capabilities of a current personal computer. Large arrays will therefore have to be solved using computer-clusters or

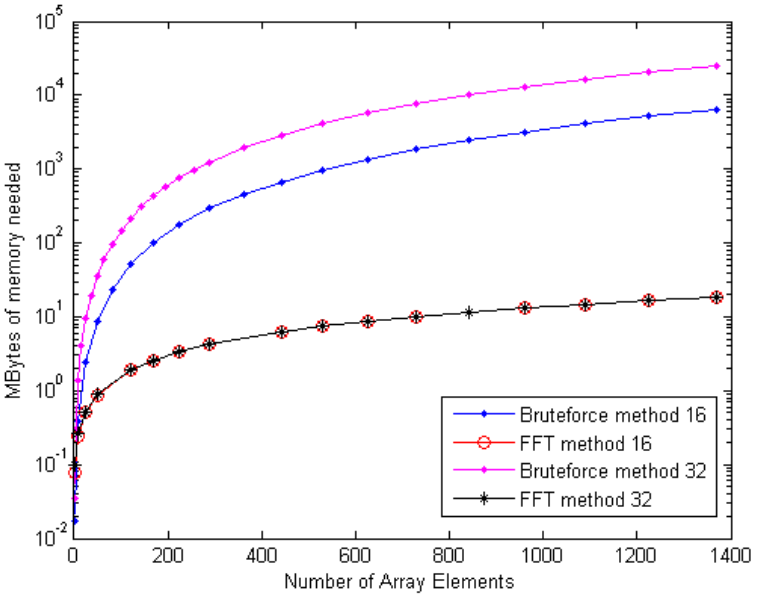

Figure 3.5: Memory Usage

super computers, which is impractical and expensive to do during the design-phase of an antenna, or when only a rough estimate of the amount of mutual coupling is required.

The results for the method using the Periodic Boundary Conditions, illustrated in Figure 3.5, show that the memory requirements comfortably stay within the range of even a substandard personal computer. Note that the y-axis is on a log-scale. As the size of the array increases, the number of basis-functions that needs solving stays constant and only the results of each new calculation has to be stored, which means that the required amount of memory will increase linearly as the number of elements in the array increase.

From these results, the improvement in memory requirements when the FFT method is used is clear. However, the trade-off in accuracy will not completely rule out brute-force MoM as a method to calculate the coupling terms of a phased array.

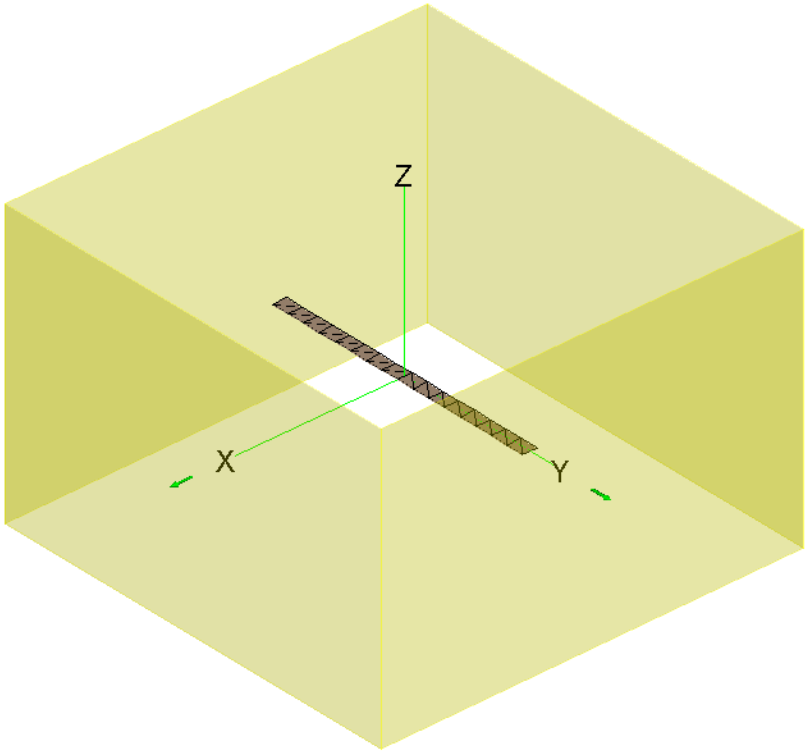

Figure 3.6: POSTFEKO View of Single Dipole Element with Period Boundary Box

3.9 Results

3.9.1 15×15 Dipole Array

The theory explained in this document was applied to calculate the coupling terms of a 15×15 element dipole array. The periodic boundary condition feature offered by FEKO was used. Figure 3.6 is that of a single element of the array as illustrated by POSTFEKO. The box in which the dipole is placed represents the size of the periodic element. The specifications of the Dipole Array are given in Table 3.1.

Firstly, the active reflection coefficient was calculated for the range of phase-differences explained above. The results were then exported to MATLAB, where the necessary data preprocessing, the FFT and then the post-processing were performed.

Figure 3.7 is the three dimensional representation of the coupling terms. The representation shows the coupling between a central element and all other elements, including the element itself. As would be expected, the element

Table 3.1: Dipole Array Parameters

Parameter	**Value**
Frequency	3 GHz
Dipole Length	0.4λ
Dipole Width	0.02λ
Spacing x-direction	0.6λ
Spacing y-direction	0.6λ

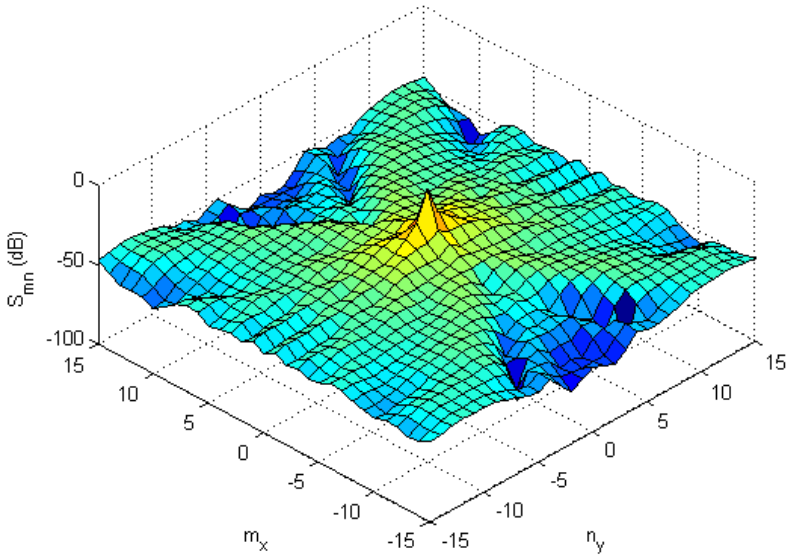

Figure 3.7: Three dimensional view of the coupling terms for a 15×15 wire dipole array

will always have the strongest coupling with itself, with values decreasing as a function of the radiation characteristics of each element, the relative separation between them and the orientation of the elements relative to each other [26]. The effect of the noise-floor can also be seen at the edges where the relative coupling start to reach values below approximately $-40dB$.

Plots depicting more precise values for the central cross-section of the array are illustrated in Figures 3.8 and 3.9. The results obtained using the PBC-MoM method are compared with those obtained using brute-force MoM. It is clear that the approximation-error is minimal for these central elements when compared to the brute-force solution. Here the effect of the noise-floor is also clear, as one would expect the decrease of the values to follow the pattern set

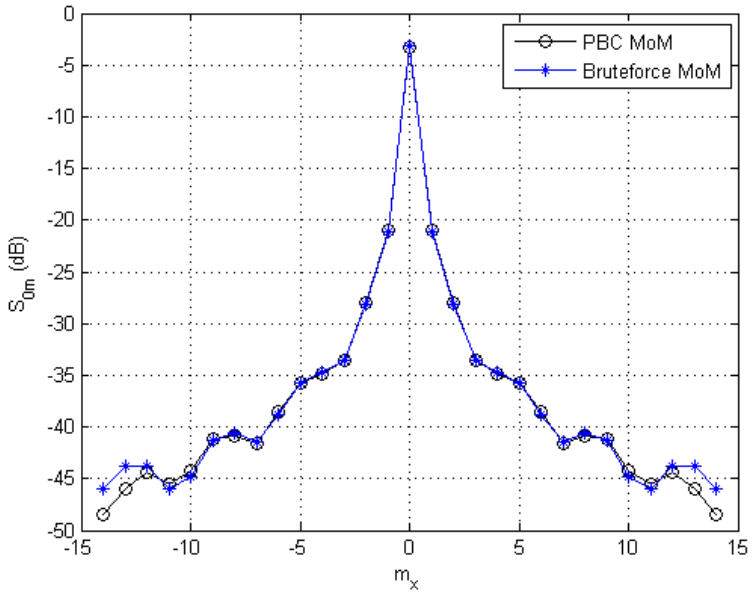

Figure 3.8: Coupling Terms along the x-axis, obtained with the PBC MoM method and the brute-force MoM method

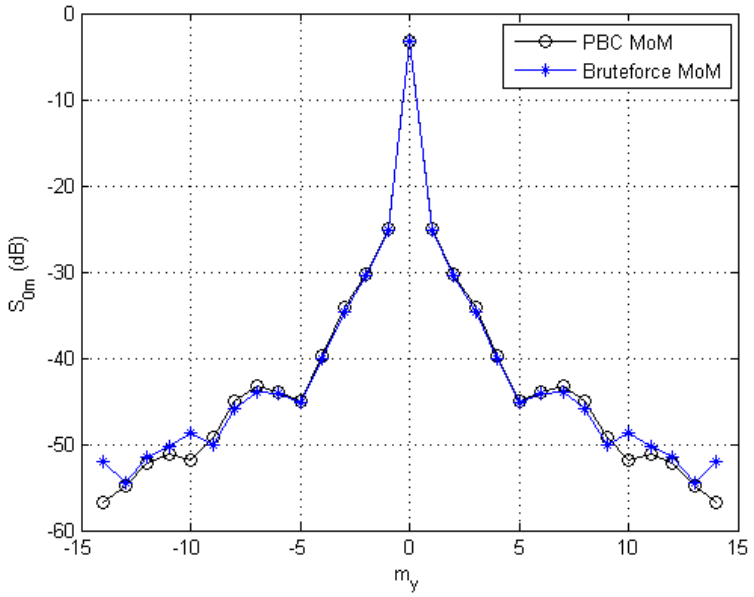

Figure 3.9: Coupling Terms along the y-axis, obtained with the PBC MoM method and the brute-force MoM method

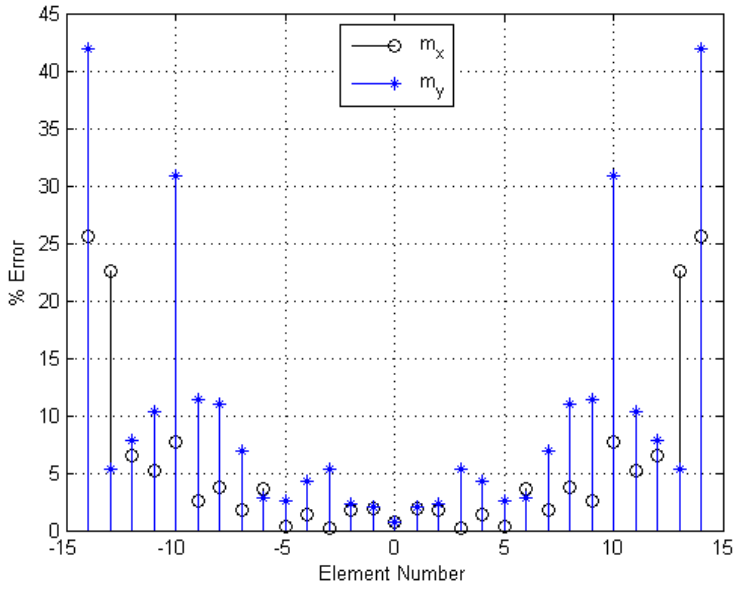

Figure 3.10: Percentage Error

by the first few values, which seems to indicate the values decreasing linearly. However, from a practical perspective, coupling below $-40dB$ is negligible.

It is important to bear in mind that these coupling terms are derived from those of an infinite array. The approximation will specifically affect the values at the edges of the array. These edge-effects will result in a higher degree of coupling calculated for the elements at the edges than the true values will be. This is because of a higher rate of scattering from the virtual elements outside the borders of the actual array.

Figure 3.10 illustrates the percentage error versus the element to which coupling has been calculated. The effects of the approximation as well as the noise-floor are clearly noticeable as the percentage error increases with distance from the centre element. As the amount of coupling decreases with distance from the centre element and approaches the noise-floor, it also adds to the error. Since there are less coupling along the y-axis, it is operating closer to the noise-floor which will increase the error along this axis.

3.9.2 8×8 Element Vivaldi Array

The following example employs Vivaldi Antennas in an array. Vivaldi antennas are widely researched for their usability as elements for Focal Plane Arrays and

Aperture Arrays. Vivaldi Arrays are also renowned for their tight coupling, which can be exploited to increase bandwidth. This makes them ideally suited for use in radio-astronomy [33].

Figure 3.11 shows the POSTFEKO model of a single Vivaldi element in its boundary box. The same procedure was followed to calculate the coupling terms as with the dipole example above.

The three dimensional results can be seen in Figure 3.12. Once again, it is clear that the strongest coupling is between the element and itself. Figures 3.13 and 3.14 illustrate the values for the coupling along the central cross-section. The coupling between the elements along the y-axis is much tighter than its counterpart along the x-axis. This is due to the elements along the y-axis being physically connected, enabling currents to flow freely between ports.

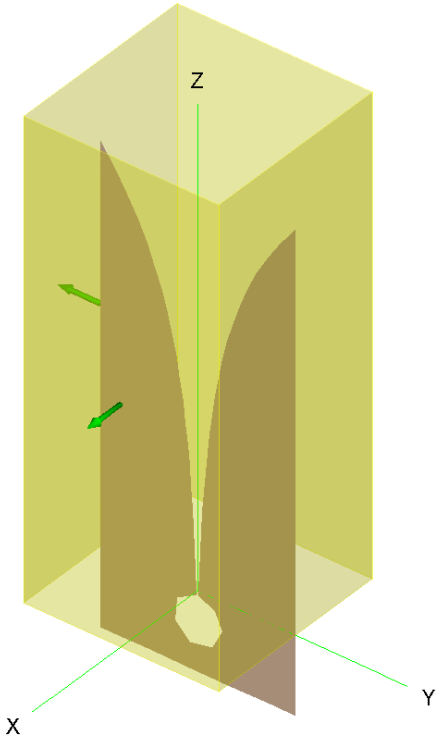

Figure 3.11: POSTFEKO view of single Vivaldi element with Period Boundary Box

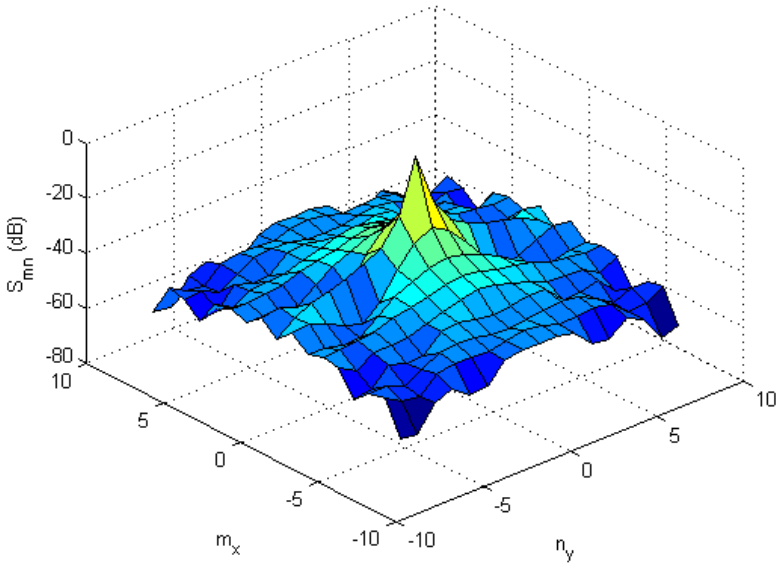

Figure 3.12: Three dimensional view of the coupling terms of a 8×8 Vivaldi array

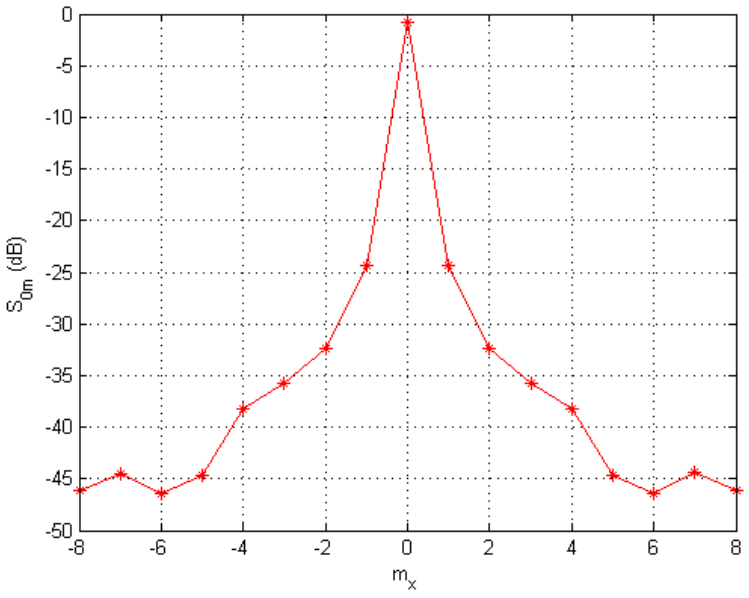

Figure 3.13: Coupling terms along x-axis

3.10 Summary

A method that can be used to calculate the mutual coupling terms in large rectangular arrays, such as Focal Plane Arrays, using infinite array analysis has been developed. An improvement in memory usage of orders of magnitude

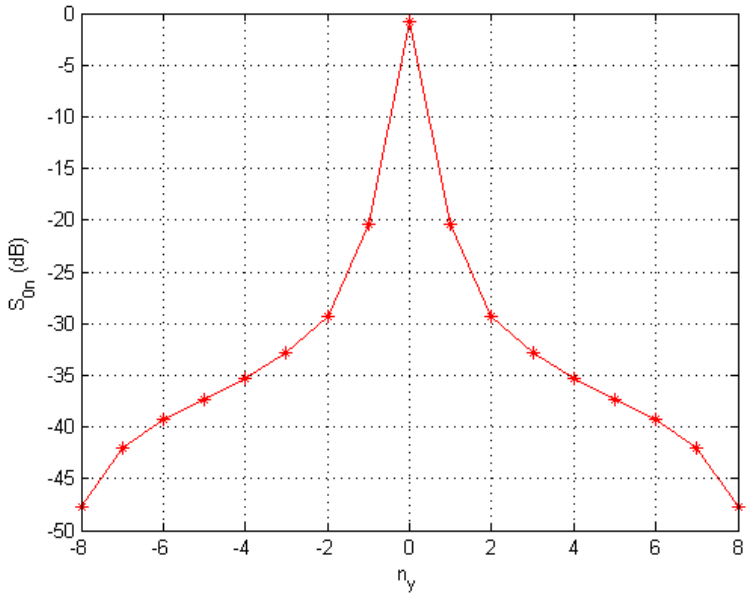

Figure 3.14: Coupling terms along y-axis

has been achieved. This improvement places the S-parameter analysis of large arrays within the range of current desktop computers. The effects of aliasing and symmetry-simplifications have also been addressed. Adequate accuracy was achieved for use during the design phase of an antenna.

Chapter 4

Noise Coupling

4.1 Introduction

As explained in Section 2.5, noise generated by the LNA's that connect the antenna array to the receiver system is not only propagated towards the receiver, but also towards the antennas. The mutual coupling between the antenna elements will result in noise power being coupled from one receiver channel to another, resulting in an additional (correlated) noise contribution. This phenomena is known as *Noise Coupling* [22]. This chapter endeavours to empirically quantify the noise coupling associated with an arbitrary system with significant mutual coupling.

In Section 4.2 a correlation matrix of an LNA noise model is given in terms of its noise parameters. In Section 4.3, an overview is given of the coupled system in a Focal Plane Array. The mutually coupled antennas and the LNA's they are connected to are represented as a single circuit diagram in order to calculate the coupled noise power. In Section 4.4, the concepts of *Active Noise Figure* and *Active Noise Temperature* are introduced. These terms are used to describe the Noise Figure or Noise Temperature of an LNA when it is connected to an antenna in an array environment. These parameters are also formulated in terms of the characteristics of the antenna array and the LNA's.

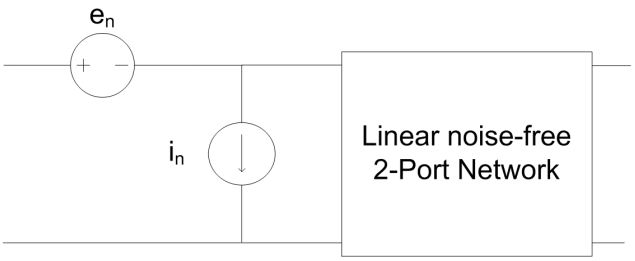

Figure 4.1: Transmission parameter noise model

4.2 The correlation matrix of an LNA in terms of its Noise Parameters

The correlation matrix derived in this section is a generic noise model describing the noise power associated with any LNA of which the noise parameters are known. The complete derivation is based on notes by Prof PW van der Walt and is given in Appendix B. The final result is summarized in this section.

Figure 4.1 shows the transmission parameter noise model of a linear two-port network. It contains a linear noise-free two-port transmission network with 2 partially correlated noise sources. The correlation matrix of the noise sources is given by

$$C = \begin{bmatrix} < e_n e_n^* > & < e_n i_n^* > \\ < i_n e_n^* > & < i_n i_n^* > \end{bmatrix}. \tag{4.2.1}$$

This can be rewritten in terms of the noise parameters of an LNA as follows

$$C_T = 2kT \begin{bmatrix} R_n & \frac{F_m - 1}{2} - R_n Y_m^* \\ \frac{F_m - 1}{2} - R_n Y_m & R_n \left| Y_m \right|^2 \end{bmatrix}, \tag{4.2.2}$$

where

- Y_m is the Optimum Source Admittance. This is the specific source admittance allowing for optimum noise match.
- F_m is the Minimum noise Figure, which is the Noise Figure resulting from optimum noise match.
- R_n is the Equivalent Noise Resistance. This is a representation in Ohm of the spectral density of a noise-voltage generator.

Section 4.3 derives a simple representative circuit diagram to describe the coupled system in terms of the scattering parameters of the array and the noise parameters of the LNA's the array elements are connected to.

4.3 Overview of the coupled system

In this section, the coupled system is discussed and simplified, and a mathematical model is derived to describe the system in terms of a simple transmission parameter model.

Figure 4.2 is an overview of the system and its equivalent circuit diagram. It consists of two antennas, both connected to an LNA. The two antennas represent an array of coupled antennas by a two-port network in the circuit diagram.

Although LNA's are considered to add little noise to a system, some noise is still generated. The circuit representation of the LNA's is that of a noiseless two-port network, with two partially correlated noise sources. Since the aim is to calculate the active noise figure of a coupled antenna array, one LNA in the system is considered a noise generator, and one antenna a noise receiver. This is a purely theoretical simplification made to calculate the amount of noise power coupled from one LNA to another via mutually coupled antennas. In practice, both LNA's act as noise generators as well as noise receivers. The noise generator (LNA j in the diagram) is therefore loaded, while the noise receiver (LNA j in the diagram) is not. The loading was only done to enable simplification of the circuit diagram. The load impedance is 50Ω, which is the assumed characteristic impedance of the network the LNA is connected to. The receiving LNA is unloaded as the noise power will be calculated in front of the noiseless two-port network to characterise the two-port noise models.

For the remainder of the chapter, the following definitions apply (refer to Figure 4.2):

ith Element	The element to which noise from the other elements is coupled.
jth Element	The element from which noise is coupled to the ith element
Coupled antennas	The antennas coupling element j with element i

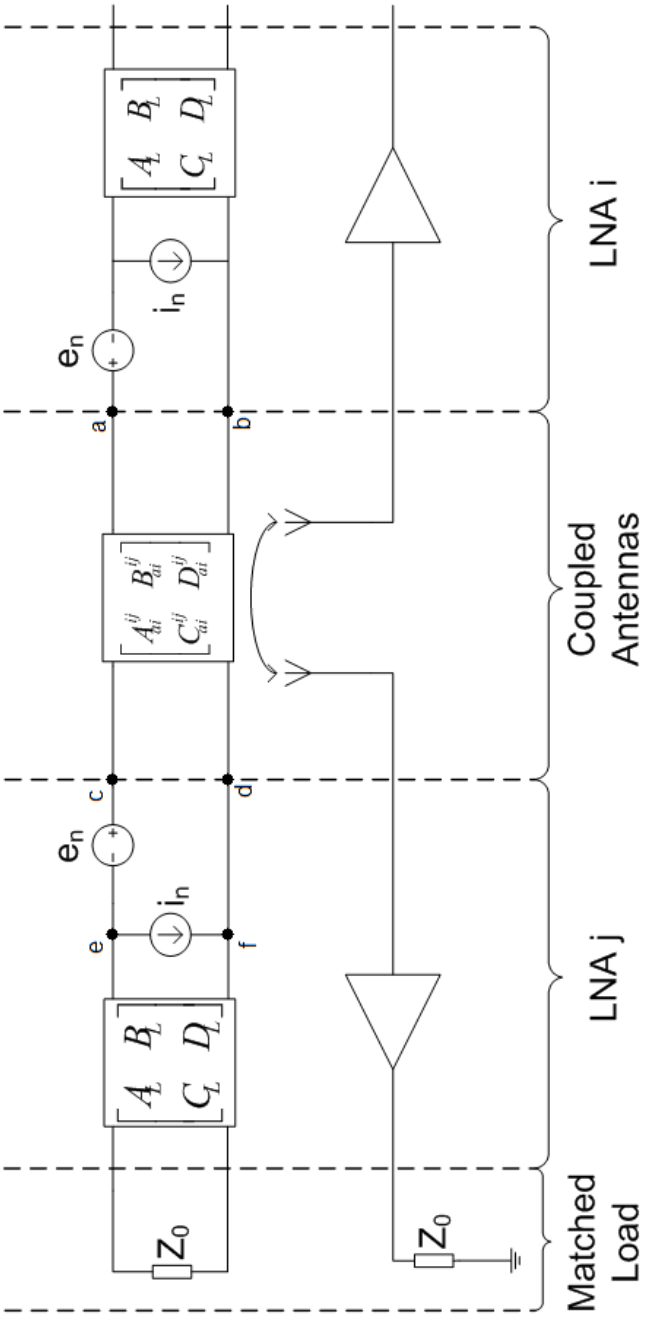

Figure 4.2: Complete circuit diagram of coupled system

4.3.1 The two-port network representing the antenna array

The two-port transmission parameter model of a multi-port antenna array is developed in this section. It is achieved by considering only two coupled antennas at a time while the other antennas are match terminated. The effect of all the coupled antennas is then combined using superposition, which necessitates the conversion of the S-parameter matrix to a range of transmission parameter matrices.

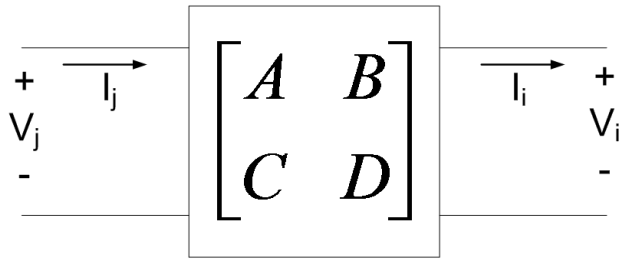

Figure 4.3: Basic Transmission parameter model

From Figure 4.3, for any two-port transmission parameter model,

$$\begin{bmatrix} V_j \\ I_j \end{bmatrix} = \begin{bmatrix} A & B \\ C & D \end{bmatrix} \begin{bmatrix} V_i \\ I_i \end{bmatrix}. \tag{4.3.1}$$

This implies that

$$\begin{aligned} V_j &= AV_i + BI_i \\ I_j &= CV_i + DI_i. \end{aligned} \tag{4.3.2}$$

For the two coupled antennas in Figure 4.4, a voltage V_j, with associated current I_j, is applied at the port of antenna j. The voltage and current received at the port of antenna i can be expressed in terms of the voltage and current at port j multiplied by a coupling term as follows:

$$\begin{aligned} V_i &= V_j S_{ij} \\ I_i &= I_j S_{ij}. \end{aligned} \tag{4.3.3}$$

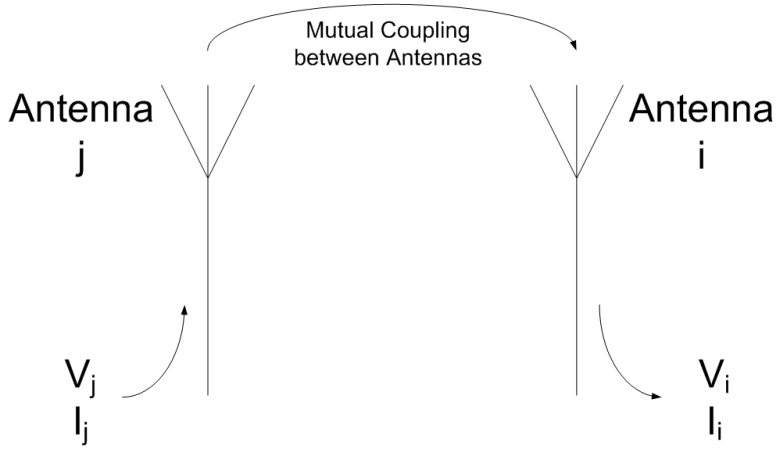

Figure 4.4: Two Coupled Antennas

Using equations (4.3.2) and (4.3.3) the two-port parameter matrix of two coupled antennas can be written as

$$\begin{bmatrix} V_j \\ I_j \end{bmatrix} = \begin{bmatrix} \frac{1}{S_{ij}} & 0 \\ 0 & \frac{1}{S_{ij}} \end{bmatrix} \begin{bmatrix} V_i \\ I_i \end{bmatrix}. \tag{4.3.4}$$

4.3.2 Simplification of the complete circuit diagram

Consider the ith element in Figure 4.2. To calculate the noise power coupled to the ith element from the other elements, the coupled antennas and the jth element is reduced to its Norton equivalent between nodes a and b on the figure, toward the antennas and element j. The reduction will be done section by section starting at the far end with loaded LNA j.

4.3.2.1 The jth Element

The loaded jth LNA can be expressed in terms of its Thevenin equivalent circuit.

First, the loaded LNA without the noise sources is expressed in terms of an input impedance as illustrated in Figure 4.5, between nodes e and f towards the load, e.g,

$$Z_{in} = \frac{AZ_0 + B}{CZ_0 + D}. \tag{4.3.5}$$

Now, the Thevenin equivalent circuit for the loaded LNA (including noise

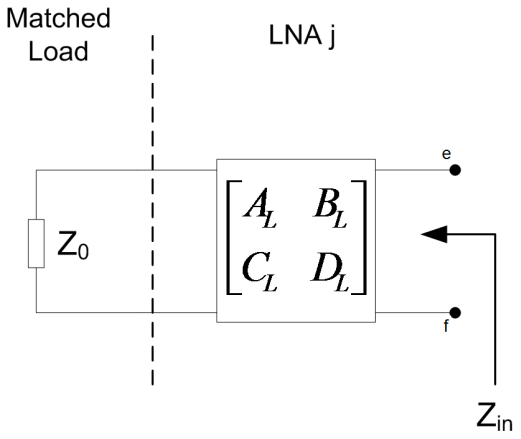

Figure 4.5: Input impedance of a loaded LNA

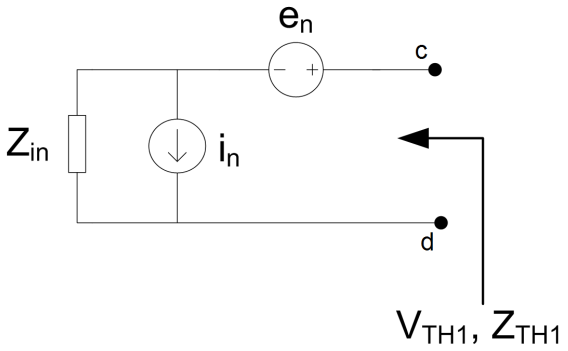

Figure 4.6: Unsolved Thevenin equivalent between nodes c and d

sources) between nodes c and d, as illustrated in Figure 4.6, is simply

$$V_{TH1} = e_n - Z_{in} i_n \tag{4.3.6a}$$

$$Z_{TH1} = Z_{in}. \tag{4.3.6b}$$

4.3.2.2 The Coupled Antennas

Next, the Thevenin equivalent of the loaded LNA is cascaded with the two-port transmission network of the coupled antennas as seen in Figure 4.7.

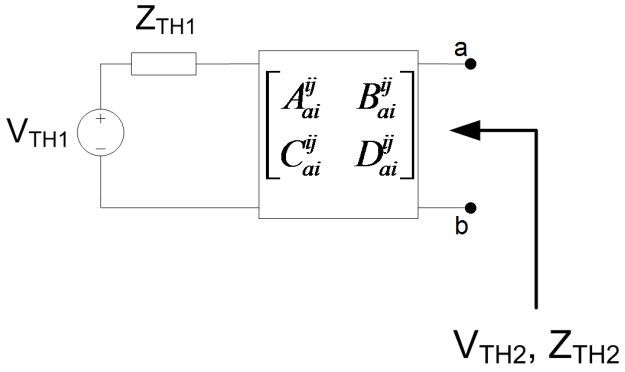

Figure 4.7: Unsolved Thevenin equivalent between nodes a and b

The Thevenin equivalent between nodes a and b is therefore

$$V_{TH2} = \frac{V_{TH1}}{A_{ai}^{ij} + B_{ai}^{ij} Z_{TH1}}, \tag{4.3.7a}$$

$$Z_{TH2} = \frac{B_{ai}^{ij} + D_{ai}^{ij} Z_{TH1}}{A_{ai}^{ij} + C_{ai}^{ij} Z_{TH1}}, \tag{4.3.7b}$$

including equations (4.3.4) and (4.3.6), it can be rewritten as

$$V_{TH2} = S_{ij} \left(e_n + Z_{in} i_n \right), \tag{4.3.8a}$$

$$Z_{TH2} = Z_{in}. \tag{4.3.8b}$$

Now, the Thevenin equivalent is converted into the Norton equivalent representing the noise generator, e.g

$$Y_N = \frac{1}{Z_{in}}, \tag{4.3.9a}$$

$$I_N = S_{ij} \left(Y_N e_n - i_n \right). \tag{4.3.9b}$$

The circuit model is used in Section 4.4 to calculate the coupled noise power.

4.4 Noise Power

In this section, the concepts of *Active Noise Figure* and *Active Noise Temperature* are introduced. These concepts are used to visualise the effect mutual coupling has on the noise temperature of a system when an element is placed within an array environment. The equivalent circuit diagram developed in the preceding sections is used to calculate the total noise coupling, since total noise coupling is one of the key parameters of the active noise figure and temperature.

4.4.1 Active Noise Figure and Active Noise Temperature

Consider an isolated antenna connected to an LNA, the noise factor of the LNA is expressed as

$$F_{isolated} = \frac{SNR_{in}}{SNR_{out}} = \frac{signal\ power\ in}{signal\ power\ out} \times \frac{noise\ power\ out}{noise\ power\ in}. \tag{4.4.1}$$

This measures the degradation of the signal to noise ratio caused by the LNA.

Now, consider a single element in an array of mutually coupled antennas. A small amount of the noise generated by the LNA's of all the other elements is coupled to that element, adding to the noise power generated by the element itself. As the extra noise power on each element is still resulting from an LNA, even though it is not the LNA connected to that element, it is not considered to be input noise power but is rather added to the output noise power. The noise factor referred to the input of the LNA is thus given by

$$F = \frac{signal\ power\ in}{signal\ power\ out} \times \frac{isolated\ noise\ power + coupled\ noise\ power}{noise\ power\ in}. \tag{4.4.2}$$

Since the noise factor, F, is referred to the input, the ratio $\frac{Signal\ power\ in}{Signal\ power\ out}$ will remain unity regardless of the signal power at the input. Consequently, the signal power added to an element as a result of mutual coupling can be ignored. The active noise factor is therefore rewritten as

$$F_{active} = F_{isolated} + F_{isolated} \times \frac{coupled\ noise\ power}{isolated\ noise\ power}, \tag{4.4.3}$$

with active noise temperature [34]

$$T_{active} = 290\,(F_{active} - 1)\,, \tag{4.4.4}$$

and active noise figure

$$NF_{active} = 10\log_{10}\,(F_{active})\,. \tag{4.4.5}$$

The active noise parameters illustrate the effect of mutual coupling on the noise performance of arrays.

4.4.2 Total Noise Coupling

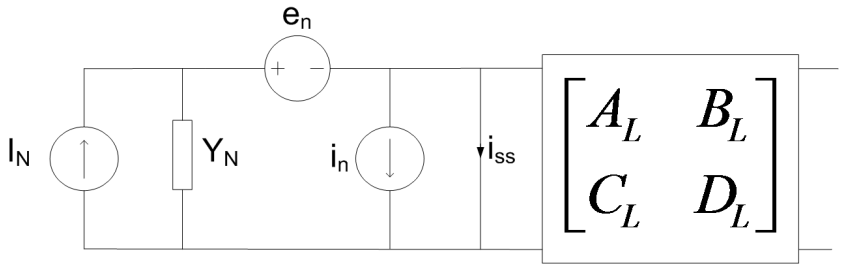

Figure 4.8: Simplified model of the coupled system

Consider Figure 4.8. The total noise power at the output of the LNA is a combination of the power contributed by all the sources. All the sources in the figure are noise sources, where I_N denotes the noise coupled to element i from element j, and the variance of I_N represents the noise power:

$$< I_N I_N^* >_{ij} = |S_{ij}|^2 < (Y_N e_n - i_n)\,(Y_N e_n - i_n)^* > . \tag{4.4.6}$$

Using superposition, the total noise power coupled from all the other elements is the sum of the noise power coupled from each of the other elements to element i, e.g

$$< I_N I_N^* >_{total} = \sum_{j \neq i} |S_{ij}|^2 < (Y_N e_n - i_n)\,(Y_N e_n - i_n)^* > . \tag{4.4.7}$$

Since the term, $< (Y_N e_n - i_n) (Y_N e_n - i_n)^* >$, is constant for all values of S_{ij}, $< I_N I_N^* >_{total}$ is rewritten as

$$< I_N I_N^* >_{total} = |S_{tot}|^2 < (Y_N e_n - i_n) (Y_N e_n - i_n)^* > . \tag{4.4.8}$$

where

$$S_{tot} = \sum_{j \neq i} |S_{ij}|^2 \tag{4.4.9}$$

Source e_n and i_n represent the noise added to the system by the isolated LNA referred to the input. As a result, the noise power of the isolated component is the variance of the component of i_{ss} contributed by these sources $(= Y_N e_n + i_n)$, e.g.

$$\begin{aligned} < (Y_N e_n + i_n) (Y_N e_n + i_n)^* > = \quad & |Y_N|^2 < e_n e_n^* > + Y_N < e_n i_n^* > \\ & + Y_N^* < i_n e_n^* > + < i_n i_n^* > . \end{aligned} \tag{4.4.10}$$

The correlation matrix for elements e_n and i_n is

$$\begin{aligned} C &= \begin{bmatrix} < e_n e_n^* > & < e_n i_n^* > \\ < i_n e_n^* > & < i_n i_n^* > \end{bmatrix} \\ &= \begin{bmatrix} C_{11} & C_{12} \\ C_{21} & C_{22} \end{bmatrix} . \end{aligned} \tag{4.4.11}$$

The correlation terms for equation (4.4.11) were derived in equation (4.2.2) in section B.3, as

$$\begin{aligned} C &= \begin{bmatrix} C_{11} & C_{12} \\ C_{21} & C_{22} \end{bmatrix} \\ &= 2kT \begin{bmatrix} R_n & \frac{F_m - 1}{2} - R_n Y_m^* \\ \frac{F_m - 1}{2} - R_n Y_m & R_n |Y_m|^2 \end{bmatrix} . \end{aligned} \tag{4.4.12}$$

For convenience, however, the correlation symbols in equation (4.4.11) will still be used.

Now, using equations (4.4.8) and (4.4.10), the ratio $\frac{coupled\ noise\ power}{isolated\ noise\ power}$ be-

comes

$$\frac{coupled\ noise\ power}{isolated\ noise\ power} = \frac{|S_{TOT}|\left(C_{11} - Y_N C_{12} - Y_N^* C_{21} + C_{22}\right)}{C_{11} + Y_N C_{12} + Y_N^* C_{21} + C_{22}}, \tag{4.4.13}$$

which is the final step required to calculate the active noise factor which is used to calculate the active noise temperature and the active noise figure. Equation (4.4.13) can now be used to calculate the active noise factor for any element in an array, e.g.

$$F_{active} = F_{isolated} + F_{isolated} \times \frac{(coupled\ noise\ power)}{isolated\ noise\ power}, \tag{4.4.14}$$

with active noise temperature referred to the input given by [34]

$$T_{active} = 290\left(F_{active} - 1\right), \tag{4.4.15}$$

and active noise figure given by

$$NF_{active} = 10\log_{10}\left(F_{active}\right). \tag{4.4.16}$$

4.5 Summary

In this chapter, a method was developed to calculate the noise coupling between elements of a mutually coupled array. This was achieved by firstly deriving the correlation matrix of the LNA in terms of its noise parameters. Then an equivalent circuit diagram was developed to represent the system of mutually coupled elements. Lastly, the terms *Active Noise Figure* and *Active Noise Temperature* were introduced and defined. These terms can be used to describe the effect mutual coupling has on the performance of an LNA when it is connected to an antenna in an array environment as opposed to being connected to an isolated antenna. This is an important consideration for tightly coupled antenna arrays used in Radio Astronomy.

In the next chapter, the formulation of this chapter is verified by means of an example. An 8×8 Vivaldi array example is also demonstrated and analysed.

Chapter 5

Implementation and Results

5.1 Introduction

In this chapter, the Active Noise Temperature (T_{active}) and Active Noise Figure (NF_{active}) for 2 examples are calculated using the method described in Chapter 4. The method was implemented using a Graphical User Interface (GUI) developed in MATLAB.

In Section 5.2, the development and usage of the GUI is discussed. In Section 5.3 a small example of a 3×3 Dipole Array is given. In this example, the change in Noise Temperature due to noise coupling was calculated using the method described in Chapter 4. The results are verified by comparing a similar calculation performed using Microwave Office. In Section 5.4 an example of an 8×8 Vivaldi Array connected to an example LNA is given. In Section 5.5 the results of the 8×8 Vivaldi Array are discussed. Section 5.6 concludes.

5.2 Graphical User Interface

A generic script with a GUI was developed in MATLAB to facilitate the calculation of T_{active} and NF_{active}. The GUI provides a straightforward interface in which the user can input the necessary information. The noise coupling is then calculated using the theory discussed in Chapter 4. In Section 5.2.1, the input required by the script is discussed, and Section 5.2.2 provides insight into the operation of the script.

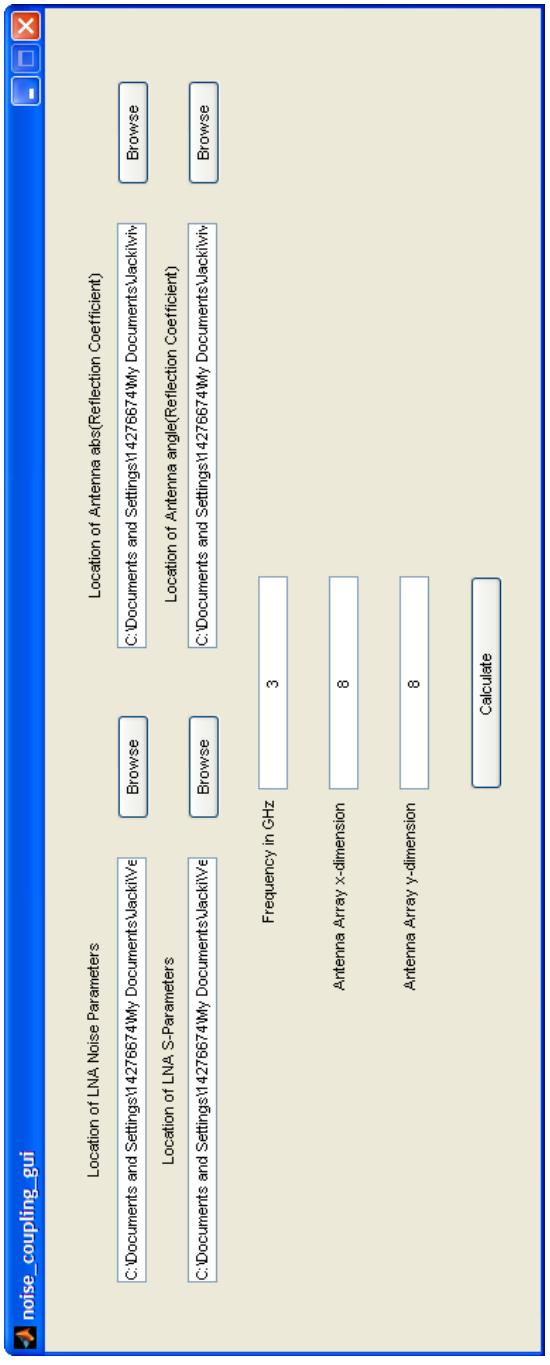

Figure 5.1: GUI Window

5.2.1 Required Input

With reference to the GUI window illustrated in Figure 5.1, the following input is required in order to calculate the Noise Coupling.

a) Location of LNA Noise Parameters and the LNA S-parameters

These refer to text files containing the noise parameters and the S-Parameters of the LNA. The files can be accessed using the "Browse" buttons located next to the editing boxes, or by manually typing the location of the file into the editing box.

The noise parameters and S-parameters of an LNA are usually given in table format in the data-sheet of the LNA. An example of a data-sheet containing both the S-Parameters and Noise-Parameters in the correct format can be seen in Appendix C. The tables in the data-sheet can be copied directly into a text file.

The format of both the Noise Parameter Table and the S-Parameter Table has to be similar to that given in Appendix C.

b) Location of Antenna abs(Reflection Coefficient) and angle(Reflection Coefficient)

This refers to the output, $\Gamma(\alpha)$, of FEKO as explained in Chapter 3.

The text file, abs(Reflection Coefficient), corresponds to $|\Gamma(\alpha)|$ and the text file angle(Reflection Coefficient) corresponds to $\angle\Gamma(\alpha)$.

Both these files are generated by exporting the results of the Active Reflection Coefficient calculation from POSTFEKO.

c) Frequency in GHz

The Frequency refers to the current operating frequency and has to correspond to the frequency used in the FEKO simulation.

Note that the frequency is specified in GHz to be compatible with the frequency ranges indicated in the LNA data-sheets. Ensure also that the selected frequency appears in both the LNA Noise Parameter table and the LNA S-parameter table.

d) Antenna Array x-dimension

The number of array elements in the x-direction.

e) Antenna Array y-dimension

The number of array elements in the y-direction.

5.2.2 Operation

The script uses the input data reviewed in Section 5.2.1, and calculates the Noise Coupling using the method discussed in Chapter 4.

The LNA Noise Parameters and S-Parameters corresponding to the desired frequency value are extracted from the input files.

The Antenna S-Parameter Matrix is calculated using the technique developed in Chapter 3 using the input files containing the $|\Gamma(\alpha)|$ and $\angle\Gamma(\alpha)$ data.

Then, all the variables in Equations (4.4.13) to (4.4.16) are calculated for all the elements in the antenna array.

Finally, figures depicting ΔT, T_{active} and NF_{active} are plotted. The figures are not part of the GUI. This enables the user to make use of MATLAB's normal Figure management capabilities.

5.3 Verification Example

In this section, the noise coupling parameters of a 3×3 Dipole Array are calculated using the method described in Chapter 4. The calculation is then repeated using Microwave Office and the resultant difference in Noise Temperature of both calculations are compared. More information on how the Microwave Office Calculation was performed is provided in Appendix D. As this example is purely for the purpose of verification, only Figure 5.5, which compares the results of the two calculations, are reviewed in this section. Figures 5.3 and 5.4, which depict the Active Noise Figure and Active Noise Temperature are therefore not discussed in detail. However, in Section 5.5, a detailed examination is made of the results pertaining to the Active Noise Figure and Active Noise Temperature.

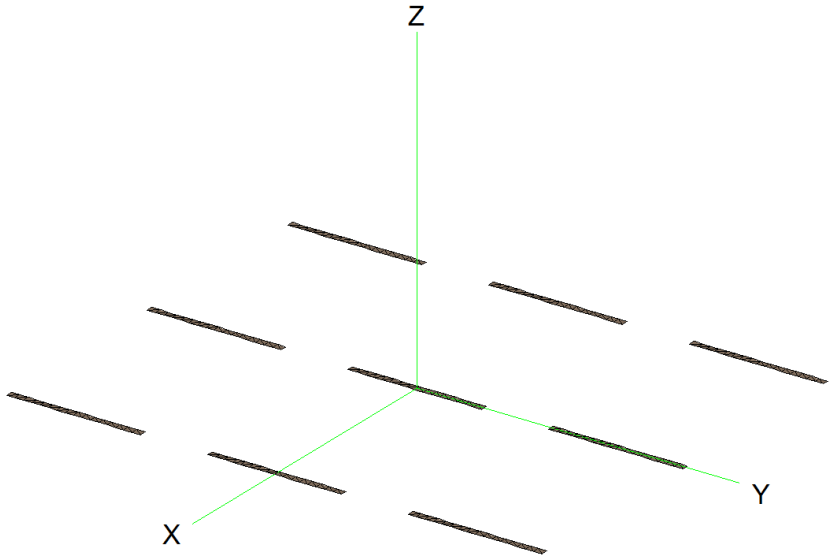

Figure 5.2: POSTFEKO Model of the 3×3 Element Dipole Array.

Table 5.1: Dipole Array Parameters

Parameter	**Value**
Frequency	3 GHz
Dipole Length	0.4λ
Dipole Width	0.02λ
Spacing x-direction	0.6λ
Spacing y-direction	0.6λ

It has been established in Chapter 3 that the FFT-method is an adequate method for calculating the coupling terms of a sufficiently large antenna array. The method will therefore not be used in this verification exercise in view of the fact that a smaller 3×3 array is used to simplify the manual calculation performed in Microwave Office, and small arrays cannot be accurately analysed using the FFT-method.

Figure 5.2 is a POSTFEKO model of the 3×3 Dipole Array. The specifications of the Dipole Array are given in Table 5.1. The parameters for the example LNA are given in Appendix C.

The comparison of the change in Noise Temperature due to noise coupling can be seen in Figure 5.5. It is clear that the results of the two calculations are an acceptable match.

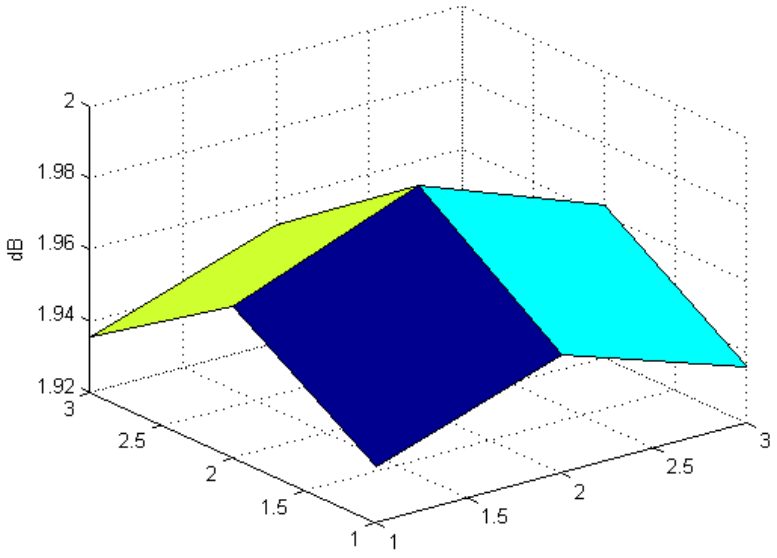

Figure 5.3: Active Noise Figure of 3×3 Element Dipole Array in dB.

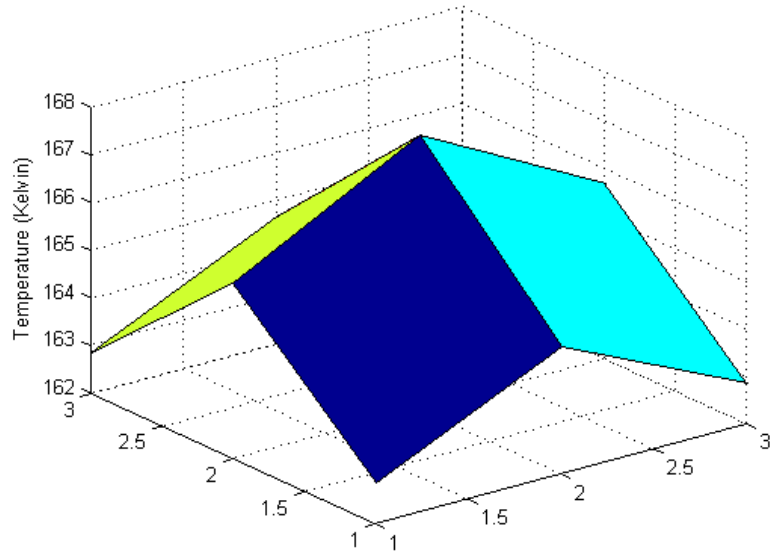

Figure 5.4: Active Noise Temperature of 3×3 Element Dipole Array in Kelvin.

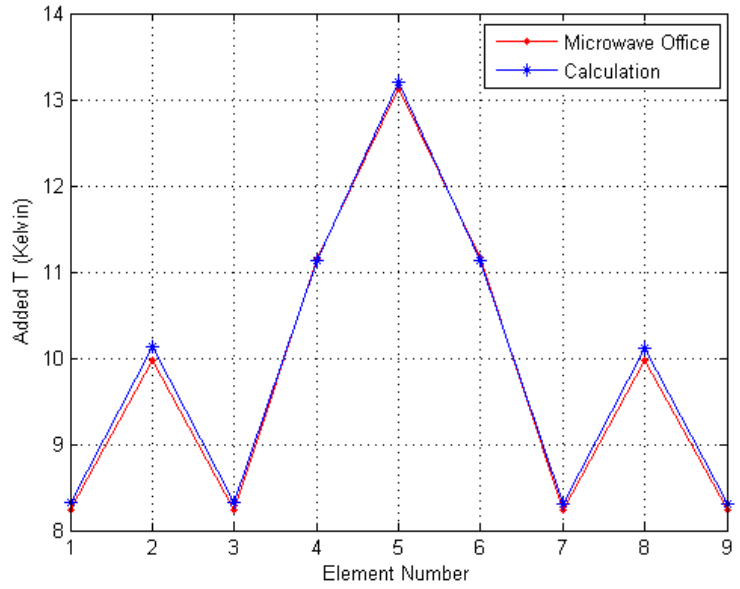

Figure 5.5: Comparison of ΔT between Microwave Office Results and Calculation Results

5.4 Vivaldi Example

The Vivaldi antenna in Figure 5.6 was simulated at $f = 0.4GHz$ using FEKO Periodic Boundary Conditions. The method explained in Chapter 3 was then used to calculate the coupling terms between the elements of the array. The results are shown in Figure 5.7. This illustrates the amount of mutual coupling between one central element and all the other elements.

It can be seen that the central element couples predominantly with itself, with coupling to neighbouring elements decreasing with distance from the central element.

After the mutual coupling terms were calculated, the active noise temperature and active noise figure were calculated for the LNA with specifications given in Table 5.2 connected to each of the elements in the 8×8 element array.

Figure 5.8 depicts the active noise temperature of the elements. The elements at the edges of the array has less noise power coupled to them than the more central elements. The active noise temperature will therefore decrease as the edges of the array are approached, with the corner-elements having the lowest active noise temperature as it has the lowest total coupling in the ar-

Table 5.2: Example Low Noise Amplifier Specifications

Symbol	Parameter	Value	Units
$NF_{isolated}$	Isolated Noise Figure	1.9	dB
$T_{isolated}$	Isolated Noise Temperature	159.1568	Kelvin
$\|S21\|$	Gain	14.2	dB
F_{min}	Minimum Noise Figure	1.61	dB
R_n	Noise Resistance	13.5	Ω
$\|\Gamma_{opt}\|$		0.28	
$\angle\Gamma_{opt}$		57.75	Degrees
$\|S_{11}\|$		0.61	
$\angle S_{11}$		-69.85	Degrees
$\|S_{21}\|$		4.66	
$\angle S_{21}$		118.37	Degrees
$\|S_{12}\|$		0.057	
$\angle S_{12}$		-16.07	Degrees
$\|S_{22}\|$		0.39	
$\angle S_{22}$		-50.92	Degrees

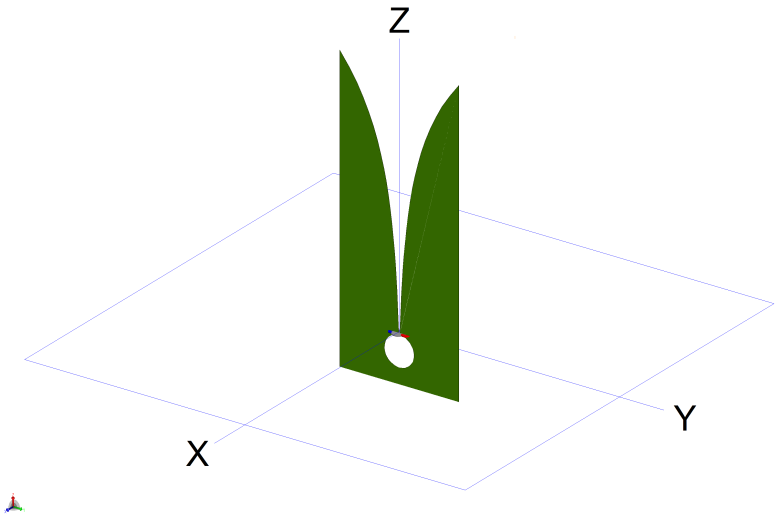

Figure 5.6: CAD model of Vivaldi element

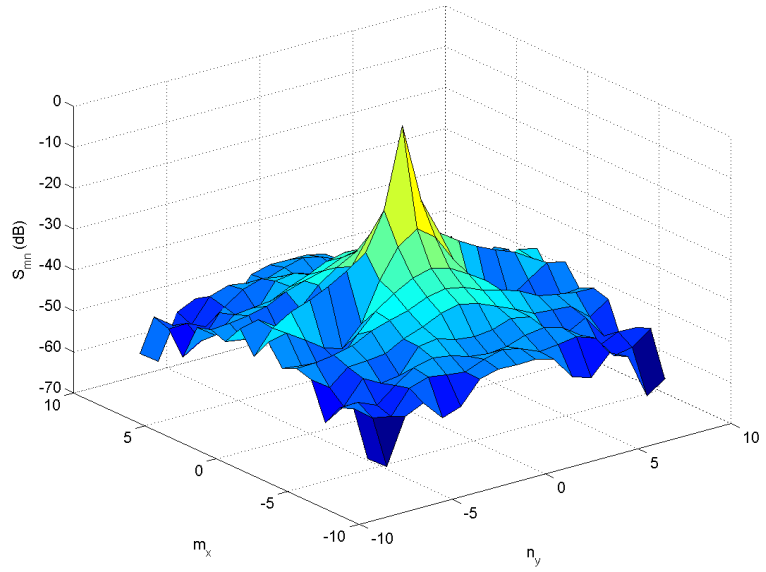

Figure 5.7: Coupling Terms between Vivaldi Array Elements (dB)

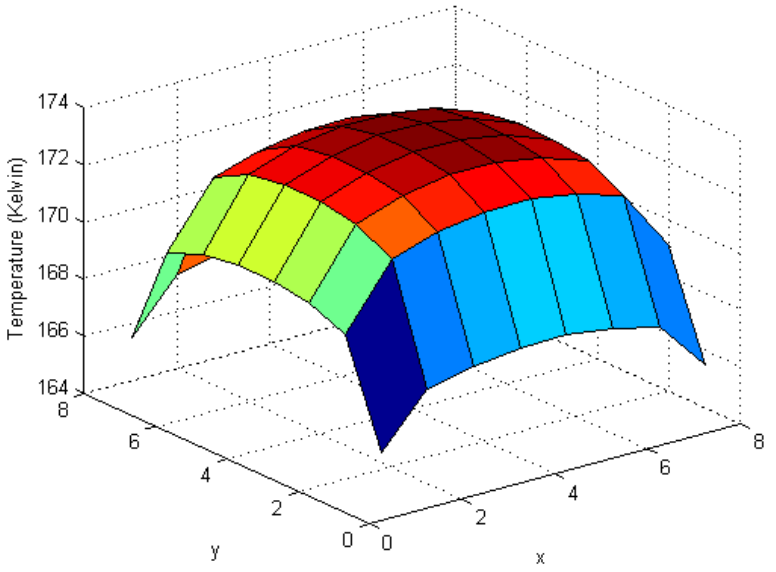

Figure 5.8: Active Noise Temperature (Kelvin)

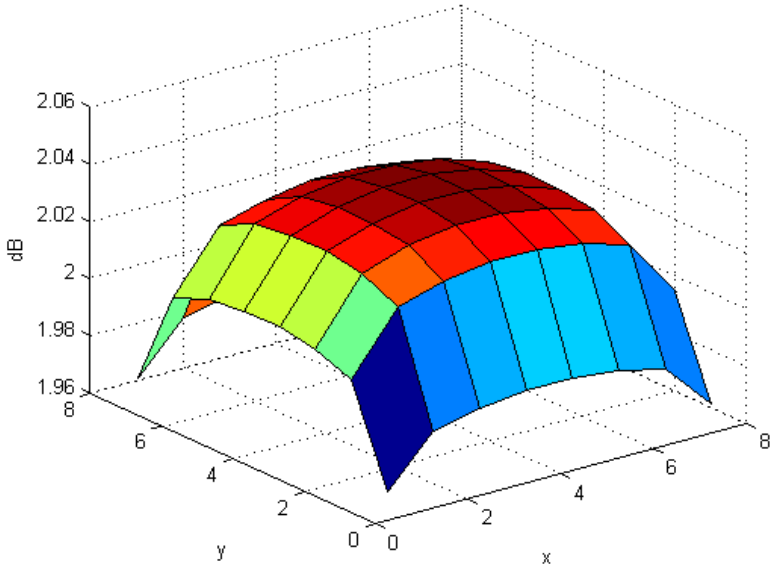

Figure 5.9: Active Noise Figure (dB)

ray. The same conclusions can be drawn from Figure 5.9, which illustrates the active noise temperature.

5.5 Discussion of Results

In the previous section, it was shown that for an 8×8 Vivaldi Array, where each antenna is connected to a reasonably noisy LNA, the maximum added noise temperature as a result of mutual coupling, was in the order of 14 Kelvin. The noise temperature of an isolated element is 159.16 Kelvin. The implies that for this LNA, there was an increase in system noise temperature of about 9%.

As mentioned in Chapter 2, system noise temperature is especially important in radio telescopes as the signals received are so weak that additional receiver noise can drown out the signal completely. This greatly reduces the usefulness of the telescope for certain areas of research.

Table 5.3 depicts the system noise temperature budget for the SKA compiled by Sandy Weinreb [35]. The maximum ΔT of the improved LNA's at 300 Kelvin will therefore be in the range of 1.3 Kelvin. From the table it can also be seen that even the smallest additions to the total system noise temperature

Table 5.3: SKA T_{sys} Budget - Current and Expected 2010 [35]

Component	**Current Technology**	**2008 Noise, K, 1.4 GHz**	**Innovation Path**	**2010 Noise, K, 1.4 GHz**
Sky	Background + atmosphere	4	No improvement here	4
Spillover & blockage	15dB edge taper + 2.5% blockage, total 4% at 300K	12	Mesh skirt for 20dB taper reduce blockage to 2%	7
Feed loss	10cm of .085; 7K + 5K feed loss	12	Twin-lead	2
LNA to feed loss	10cm of 0.141 Cu coax bend to dewar, 0.04dB at 300K	3	40mm twin-lead	2
Vacuum feedthru	Glass/Kovar bead, 0.1dB	7	Quartz/gold, 0.04dB	3
Coax in dewar	10cm or 0.141 SS/BeCu 0.03dB at 190K	4	Air line	2
Coupler at 70K	Werlatone C7753, 0.2dB	3	or noise lamp coupling	2
Total	Total above	45	Total above	25
LNA 300K	Commercial 0.5 to 4 GHz LNA	35	Improved LNA 300K	15
LNA 60K	Current LNA	14	Improved 70K LNA	5
	Total T_{sys}, 300K LNA	**80**	**Total T_{sys}, 300K LNA**	**40**
	Total T_{sys}, 60K LNA	**59**	**Total T_{sys}, 60K LNA**	**30**

are taken into account. This highlights the prominence of even an additional 1.3 Kelvin to the system noise temperature. Consequently, the research on noise coupling documented in this thesis, is significant in the context of the SKA.

Table 5.4: Estimate ΔT versus First Term Coupling and T_{LNA}

$S_{0,1}$ \ T_{LNA}	15 K	30 K	80 K	159.2 K	290 K
-3 dB	72.8 K	145.7 K	388.5 K	772.9 K	1408 K
-10 dB	14.5 K	29.1 K	77.5 K	154.2 K	281 K
-15 dB	4.6 K	9.2 K	24.5 K	48.8 K	88.9 K
-20 dB	1.5 K	2.9 K	7.8 K	15.4 K	28.1 K
-20.47 dB	1.3 K	2.6 K	7.0 K	13.8 K	25.2 K
-25 dB	0.46 K	0.92 K	2.5 K	4.9 K	8.9 K

In Table 5.4, estimated values of maximum noise temperature increase due to mutual coupling in an 8×8 array can be seen. Various values of LNA noise temperatures (T_{LNA}) are represented, as well as various values of first term coupling ($S_{0,1}$). This table can be used as a quick reference guide to estimated noise coupling penalty. Note, however, that the values in the table are merely projected values for an 8×8 array. This implies that the theory developed in Chapter 4 will still need to be applied in order for the necessary accuracy to be preserved.

5.6 Summary

In this chapter, the theory explained in the previous chapters was implemented by means of a Graphical User Interface (GUI).

Instructions were given on how the GUI should be used which included information on all the required input. Furthermore, the basic functionality of the script was explicated.

In Section 5.3, the method for calculating the noise coupling in a large antenna array as explained in Chapter 4, were verified by comparing the results with a similar calculation done using Microwave Office. The example used for verification was a 3×3 dipole array.

In Section 5.4, the noise coupling of an 8×8 Vivaldi Array was calculated using the method explained in Chapter 4.

The significance of the results in the context of radio astronomy was discussed in Section 5.5. A quick reference table for noise coupling penalty in an 8×8 array was also compiled in this section.

Chapter 6

Conclusions and Recommendations

6.1 Conclusions

In an array of antennas, several factors influence the mutual coupling between the elements of the array. One of these factors is the relative spacing between the elements of the array. Sparse arrays will have relatively low mutual coupling, while in dense arrays, the mutual coupling will be more pronounced. Focal Plane Arrays (FPA's) were introduced in Section 2.4, and are by definition large and densely packed. This results in a high level of mutual coupling.

The effect of mutual coupling on the overall performance of phased arrays poses more problems than only those described in Section 3.1. Each antenna in the array is also connected to an LNA generating a small amount of noise. Noise power generated by the LNA's do not only travel toward the receiver circuitry, but also back towards the antenna, from where it is radiated and also received by the other antennas in the array. This phenomenon is referred to as *Noise Coupling*.

The terms *Active Noise Figure* and *Active Noise Temperature*, which were introduced in Section 4.4.1, describe the noise behaviour of the system as a result of noise coupling. The active noise figure (NF_{active}) and active noise temperature (T_{active}), are dependent on two factors:

(a) The mutual coupling terms of the antenna array,

(b) The noise power generated by an isolated LNA.

The two factors are combined to calculate the noise power coupled to each element of the array from all the other elements. The coupled noise power is then used to calculate NF_{active}, and T_{active}, which are parameters that describe the effect mutual coupling has on the noise performance of antenna arrays, using the following equations derived in Chapter 4:

$$F_{active} = F_{isolated} + F_{isolated} \times \frac{coupled\ noise\ power}{isolated\ noise\ power}, \tag{6.1.1}$$

with active noise temperature [34],

$$T_{active} = 290\,(F_{active} - 1)\,, \tag{6.1.2}$$

and active noise figure,

$$NF_{active} = 10\log_{10}(F_{active})\,. \tag{6.1.3}$$

In this research, two main problems were therefore addressed. The first being the calculation of the mutual coupling in large phased arrays, and the second the calculation of the noise coupling.

6.1.1 Mutual coupling

As mentioned previously, FPA's are large arrays that are densely packed. Two candidate elements are currently being investigated for use in FPA applications (see Section 2.4). These are the Vivaldi Element (Vivaldi Array), and a corner-fed patch antenna (Checkerboard Array).

The analysis of large arrays using simulation packages such as FEKO or CST, are memory intensive. To solve FPA's using brute-force methods are therefore an impossible task using current desktop computers. Consequently, another method which greatly reduces the memory requirements is needed.

In Chapter 3 infinite array analysis is used to calculate the coupling terms of an antenna array. This enables the use of a periodic boundary condition feature offered by both FEKO and CST. The computer therefore only has to analyse a single element, regardless of the size of the array, which places the S-parameter analysis of large arrays comfortably within the range of current desktop computers.

The effects of aliasing and symmetry-simplifications are also addressed. Adequate accuracy was achieved for use during the design phase of an antenna, or when only a good estimation is necessary. It should be noted that in essence, the method approximates a large array as an infinite one, and therefore edge-effects are ignored. This implies that the accuracy improves as the size of the array increases. The method is therefore not applicable for use in smaller arrays.

6.1.2 Noise Coupling

In Sections 2.2 and 2.3, basic functionality and use of radio telescopes, and factors influencing the sensitivity were discussed. Among these factors was receiver noise, which was discussed in further detail in Section 2.3.2. The importance of a low receiver noise temperature was also emphasized.

Section 2.5 introduces the problem of noise coupling with reference to previous studies done on the subject. It was seen that although the importance of noise coupling was highlighted, not much literature is available proposing a method with which it can be calculated.

In Chapter 4, a method to calculate the noise coupling between elements of a mutually coupled array was developed. This was achieved by firstly deriving the correlation matrix of the LNA in terms of its noise parameters. Then an equivalent circuit diagram was developed to represent the system of mutually coupled elements. Lastly, the terms *Active Noise Figure* and *Active Noise Temperature* were defined. These terms can be used to describe the effect mutual coupling has on the performance of an LNA when it is connected to an array of mutually coupled antennas. This is an important consideration for tightly coupled antenna arrays currently begin proposed to be be used in radio telescopes.

6.2 Contributions

Based on the work presented in Chapters 2 to 5, the contributions of this research can be listed as follows:

1. The term *active reflection coefficient* was defined and discussed.

2. Infinite array theory was used to derive a method with which the coupling terms of a large finite phased array can be estimated. This method enables the use of periodic boundary conditions to calculate the S, Z and Y parameter matrices, which greatly improves memory usage. The method was named the *FFT-method*.

3. An application of symmetry to reduce the run time of the FFT-method was discussed.

4. Aliasing considerations regarding the FFT-method were discussed and a solution proposed to mitigate the effects aliasing has on the accuracy of the calculation.

5. Performance in terms of memory usage displayed by the FFT-method was compared to that of the traditional brute-force MoM method.

6. A two-port noise model was derived to represent an LNA in terms of its noise parameters.

7. An equivalent circuit diagram was developed to characterise the entire system of coupled elements.

8. The terms *Active Noise Figure* (NF_{active}) and *Active Noise Temperature* (T_{active}) were introduced to describe the effect of mutual coupling on the noise performance of antenna arrays.

9. A generic expression was deduced which can be used to calculate the total noise power coupled to an element in an array of mutually coupled antennas. The expression is in terms of the measurable noise parameters of an LNA, and the S-parameters of the antenna array.

10. A generic expression was deduced to calculate NF_{active} and T_{active}.

11. A graphical user interface was developed using MATLAB to simplify the calculation of ΔT, NF_{active} and T_{active}.

12. A quick reference guide of estimated noise coupling penalty was compiled. Values of ΔT are tabled against various values of LNA noise temperature (T_{LNA}) and first term coupling ($S_{0,1}$).

6.3 Recommendations and Future Work

a) Alleviation of edge-effects resulting from the infinite array approximation

The FFT-method developed in Chapter 3 is an effective method that can be used to estimate the coupling terms of a large phased array. In effect, the method approximates a large array as an infinite array, thereby ignoring the edge-effects. If a technique can be developed to alleviate the edge-effects, the accuracy of the solution of an array of any size and geometry will be comparable to that of a brute-force calculation. It will therefore be possible to do high-accuracy design of large antenna arrays on a current desktop computer.

b) Proper Parallel Implementation of the FFT-method

Currently, most desktop computers have at least two CPU-cores. In theory, the total number of instructions are divided between the cores and executed simultaneously, shortening the time needed to execute the set of instructions by a factor related to the number of cores in the CPU.

In practice, however, the overhead communication due to exchange of data between the cores also adds to the processing time. If the cores exchange data frequently, the parallel implementation becomes ineffective, which can eventually actually slow down the calculation instead of speeding it up.

When using the FFT-method, the active reflection coefficient is calculated repeatedly with only the phase-shift changing. Each calculation is therefore independent of the others. Since only a single element in the array is being analysed with each repetition, the instantaneous memory requirements for two cores will still only be that of two elements, which should not exceed the total available memory.

At the moment, the “for-loop” used in FEKO and the “parameter-sweep” used in CST do not take into account that the repetitions are independent of one another. When running a parallel calculation, only the analysis of the structure is parallelised, requiring a lot of data-exchange between cores. This is very ineffective. It would be much more effective to parallelise the loop structures, which require no interim data-exchange.

This proper implementation of the FFT-method will greatly reduce the CPU-time needed to run the analysis.

c) Mitigation of Noise Coupling in Focal Plane Arrays

In Section 2.5 the importance of the analysis of noise coupling in FPA's for use in radio telescopes are emphasised. The noise coupling and the overall effect it has on the noise performance of the array was discussed in this document.

The next step would be to investigate methods that can be used to minimize the noise coupling. Since the high level of mutual coupling in FPA's are being exploited to improve the overall bandwidth of the array [33], merely improving the mutual coupling by proper impedance matching techniques should therefore be avoided.

Appendices

Appendix A

SKA Specifications

The final design of the SKA will be determined by the outcome of the extensive prototyping and costing exercise currently under way. The specifications of the reference design for frequencies up to 10GHz are given in Table A.1.

Table A.1: SKA Specifications

Parameter	**Specification**
Frequency range	70 MHz to 10 GHz
Sensitivity (area / system temperature)	5,000 m^2/K (400 ìJy in 1 min) between 70 and 300 MHz, 10,000 m^2/K (200 ìJy in 1 min) between 0.3 and 10 GHz
Survey figure-of-merit	$4 \times 10^7 \rightarrow 3 \times 10^9$ m^4k^{-2} deg^2 depending on sensor technology and frequency
Field-of-view	200 square degrees between 70 and 300 MHz; $\geq$30 square degrees between 0.3 and 1 GHz 1 square degree maximum between 1 and 10 GHz
Angular resolution	<0.1 arcsecond
Instantaneous bandwidth	25% of band centre
Spectral (frequency) channels	16,384 per band per baseline
Calibrated polarization purity	10 000:1
Synthesized image dynamic range	>1,000,000
Imaging processor computation rate	10^{15} operations/second
Telescope output data rate	1 TByte per minute (typical)

Appendix B

Derivation of the Correlation Matrix of an LNA in terms of its Noise Parameters

This appendix contains the derivation of the correlation matrix of an LNA in terms of its noise parameters. The derivation is used in Chapter 4 to calculate the noise coupling in an antenna array. The formulation is based on notes by Prof PW van der Walt [36].

B.1 The Correlation Matrix of Noise Signals

In this section, the correlation matrix of a noise signal is derived.

For this derivation, all noise signals are considered to be band limited around a frequency f_0 and are represented by phasors with randomly varying amplitude, A, and phase, ϕ, e.g.

$$i(t) = A(t)e^{j(2\pi f_0 t + \phi(t))}, \tag{B.1.1}$$

therefore linking the time and frequency domains.

The variance of a noise signal is given by the time average,

$$p \rightarrow \sigma^2 = \lim_{T\rightarrow\infty} \frac{1}{2T} \int_{-T}^{T} i(t)i^*(t)dt =< ii^* >=< A^2 >, \tag{B.1.2}$$

where T, denotes the period over which the average is calculated. The time

average also represents the power spectral density per unit bandwidth of the signal at the frequency f_0. The integral in equation (B.1.2) can also be recognised as the autocorrelation if $i(t)$ with zero time shift, $R(0)$.

For convenience, the variance (or rms^2 value) of a noise voltage or current in one unit bandwidth is expressed in terms of an equivalent noise resistance, e.g.

$$\begin{aligned} < ee^* > &= 2kTR_n, \\ < ii^* > &= 2kTG_n, \end{aligned} \tag{B.1.3}$$

with k being Boltzmann's constant, and T the temperature in Kelvin. Since the variance is an even function symmetrical around zero, only the positive side of the spectrum is taken into account. The functions are therefore multiplied by a factor of two to account for the negative frequencies.

Now, consider two partially correlated noise signals: $e = e(t)$ and $i = i(t)$. For convenience, one of the signals will be split into its correlated and uncorrelated parts:

$$i = i_u + i_c = i_u + Y_c e. \tag{B.1.4}$$

The noise conductance is also split into its correlated and uncorrelated parts as follows:

$$G_n = G_c + G_u. \tag{B.1.5}$$

The cross-correlations are therefore expressed as

$$\begin{aligned} < ei^* > &= 0, \\ < ei_c^* > = < ei^* > &= Y_c^* < ee^* >, \end{aligned} \tag{B.1.6}$$

and autocorrelations as

$$\begin{aligned} < ee^* > &= 2kTR_n, \\ < ii^* > = < (i_u + i_c)(i_u + i_c)^* > &= 2kT\left(G_u + |Y_c| R_n\right). \end{aligned} \tag{B.1.7}$$

This yields the correlation matrix,

$$\begin{aligned} C &= < \begin{bmatrix} e \\ i \end{bmatrix} . \begin{bmatrix} e & i \end{bmatrix}^* > \\ &= < \begin{bmatrix} ee^* & ei^* \\ e^*i & ii^* \end{bmatrix} > \\ &= 2kT \begin{bmatrix} R_n & R_n Y_c^* \\ R_n Y_c & G_u + R_n |Y_c|^2 \end{bmatrix}. \end{aligned} \tag{B.1.8}$$

B.2 Optimum source admittance

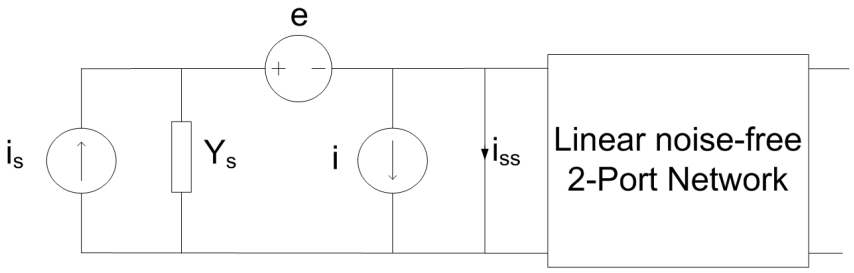

Figure B.1: Model of a two-port driven by a source with admittance Y_s

The aforementioned noisy two-port network can now be characterised by a noise voltage source and a noise current source connected to the input of a noiseless two-port network as illustrated in Figure B.1. Should the voltage source, e, be the dominant source, the transmission noise signal can be minimized using a high source impedance, Y_s. Should the current source, i, be the dominant source, a low transmission noise signal can be obtained using a low source impedance. When both the sources are present, there exists a specific source admittance (or impedance) that allows for a minimal noise propagation from the noise sources. This specific source admittance is referred to as the *Optimum Source Admittance*, and results in an *Optimum Noise Match*. The noise figure resulting from an optimal noise match is then referred to as the *Minimum Noise Figure* [37].

Figure B.1 illustrates the model of a noisy two-port network driven by a source with admittance Y_s.

Let the current noise component contributed by the source conductance, G_s, be denoted by i_n. The total noise component of i_{ss}, with noise contributions from i_n, e and i, is given by:

$$i_{ss} = i_n + Y_s e + i. \tag{B.2.1}$$

The system noise factor is defined by the ratio,

$$F = \frac{\left.\frac{signal\ power}{noise\ power}\right|_{in}}{\left.\frac{signal\ power}{noise\ power}\right|_{out}}. \tag{B.2.2}$$

When the power-ratios for i_{ss} is compared in front of the two port, this definition simplifies to

$$F = \frac{noise\ power\ out}{noise\ power\ in}, \tag{B.2.3}$$

where *"noise power in"* is the variance of i_n ($< i_n i_n^* >= 2kTG_s$), and *"noise power out"* is the variance of i_{ss} described in equation (B.2.1). Note that the noise of the source and the noise of the noise sources are uncorrelated. The noise factor is therefore expressed as

$$\begin{aligned} F &= \frac{< i_n i_n^* > + < (Y_s e + i)(Y_s e + i)^* >}{< i_n i_n^* >} \\ &= 1 + \frac{< (Y_s e + i)(Y_s e + i)^* >}{< i_n i_n^* >}. \end{aligned} \tag{B.2.4}$$

With

$$\begin{aligned} < (Y_s e + i)(Y_s e + i)^* > &= < \left(\begin{bmatrix} Y_s & 1 \end{bmatrix} \begin{bmatrix} e \\ i \end{bmatrix} \right) \left(\begin{bmatrix} e & i \end{bmatrix} \begin{bmatrix} Y_s \\ 1 \end{bmatrix} \right)^* > \\ &= \begin{bmatrix} Y_s & 1 \end{bmatrix} C \begin{bmatrix} Y_s^* \\ 1 \end{bmatrix}, \end{aligned} \tag{B.2.5}$$

where C is the correlation matrix of the two noise sources.

Incorporating equations (B.1.8),(B.2.4) and (B.2.5), the noise factor is

$$F = 1 + \frac{(G_s^2 + 2G_c G_s + G_c^2 + B_s^2 + 2B_c B_s + B_c^2)\, R_n + G_u}{G_s}. \tag{B.2.6}$$

By differentiating F with respect to G_s and B_s and setting the derivatives

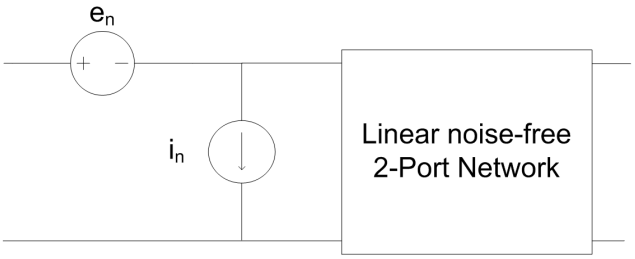

Figure B.2: Transmission parameter noise model

to zero, the optimum source admittance, $Y_{s,opt} = Y_m = G_m + jB_m$, is found.

From

$$\frac{\partial F}{\partial B_s} = \frac{2\left(B_s + B_c\right) R_n}{G_s} = 0 \tag{B.2.7}$$

the optimum source susceptance B_m is given as

$$B_m = -B_c. \tag{B.2.8}$$

With

$$\frac{\partial F}{\partial G_s} = \frac{\left(G_s^2 - G_c^2 - B_s^2 - 2B_cB_s - B_c^2\right) R_n - G_u}{G_s^2} = 0, \tag{B.2.9}$$

and substituting $B_s = -B_m$, it follows that

$$G_m = \sqrt{G_c^2 + \frac{G_u}{R_n}}. \tag{B.2.10}$$

The minimum Noise Figure is therefore given by

$$F_m = 1 + 2R_n\left(G_c + \sqrt{G_c^2 + \frac{G_u}{R_n}}\right). \tag{B.2.11}$$

In the next section, a method is derived to express the correlation matrix of an LNA in terms of its noise parameters.

B.3 Two-port noise models

Figure B.2 shows the transmission parameter noise model of a linear two-port network.

From sections B.1 and B.2, the correlation matrix, C_T and the minimum Noise Figure, F_m, with a source admittance $Y_m = G_m + jB_m$ are attained as follows:

$$C = 2kT \begin{bmatrix} R_n & R_n Y_c^* \\ R_n Y_c & G_u + R_n |Y_c|^2 \end{bmatrix}, \tag{B.3.1}$$

$$G_m = \sqrt{G_c^2 + \frac{G_u}{R_n}} \tag{B.3.2}$$

$$B_m = -B_c \tag{B.3.3}$$

$$F_m = 1 + 2R_n \left(G_c + \sqrt{G_c^2 + \frac{G_u}{R_n}} \right). \tag{B.3.4}$$

The noise parameters F_m, $Y_m = G_m + jB_m$ and R_n can be determined by measurements or are displayed on the data sheet of the component. The elements of the correlation matrix are then found by solving equations (B.3.2) through (B.3.4) for G_u and Y_c as follows:

$$G_u = \frac{(4F_m - 4)\, G_m R_n - F_m^2 + 2F_m - 1}{4R_n}, \tag{B.3.5}$$

$$Y_c = \frac{-2G_m R_n + F_m - 1}{2R_n} - jB_m. \tag{B.3.6}$$

After substituting the above expressions for G_u and Y_c into equation (B.3.1), the correlation matrix is expressed in terms of the noise parameters as follows:

$$C_T = 2kT \begin{bmatrix} R_n & \frac{F_m - 1}{2} - R_n Y_m^* \\ \frac{F_m - 1}{2} - R_n Y_m & R_n |Y_m|^2 \end{bmatrix}. \tag{B.3.7}$$

The correlation matrix derived in this section is a generic noise model describing the noise power associated with any LNA of which the noise parameters are known.

Appendix C

S-Parameter and Noise Parameter Tables as Given in the Data-sheet of an Example LNA

MGA-52543 Typical Scattering Parameters

T_C = 25°C, V_d = 5.0 V, I_d = 53 mA, Z_0 = 50 Ω, (from S and Noise Parameters in ICM test fixture)

Freq	s_{11} (m)	s_{11} (a)	s_{21} (dB)	s_{21} (m)	s_{21} (a)	s_{12} (dB)	s_{12} (m)	s_{12} (a)	s_{22} (m)	s_{22} (a)	K
0.2	0.64	-17.42	14.92	5.57	168.30	-22.90	0.072	16.89	0.53	-14.49	1.00
0.3	0.62	-18.44	14.76	5.47	166.18	-22.62	0.074	9.26	0.51	-15.38	1.04
0.4	0.61	-20.41	14.67	5.41	163.57	-22.56	0.074	4.62	0.51	-17.35	1.06
0.5	0.60	-23.21	14.60	5.37	160.09	-22.58	0.074	0.54	0.49	-18.04	1.08
0.6	0.60	-26.02	14.54	5.33	156.98	-22.66	0.074	-2.26	0.48	-20.59	1.09
0.7	0.60	-29.01	14.46	5.28	153.79	-22.78	0.073	-4.58	0.48	-23.14	1.10
0.8	0.60	-31.88	14.37	5.23	150.67	-22.92	0.071	-6.59	0.47	-25.89	1.12
0.9	0.60	-35.42	14.28	5.18	147.57	-23.06	0.070	-8.26	0.46	-28.24	1.13
1	0.60	-38.48	14.19	5.13	144.53	-23.23	0.069	-9.68	0.45	-31.05	1.14
1.1	0.60	-41.81	14.10	5.07	141.44	-23.40	0.068	-10.91	0.44	-33.35	1.16
1.2	0.61	-45.23	14.01	5.02	138.48	-23.58	0.066	-12.02	0.44	-35.96	1.17
1.3	0.61	-48.69	13.92	4.96	135.50	-23.76	0.065	-13.01	0.43	-38.26	1.19
1.4	0.61	-52.14	13.82	4.91	132.59	-23.95	0.063	-13.77	0.42	-40.57	1.21
1.5	0.61	-55.73	13.73	4.86	129.67	-24.14	0.062	-14.46	0.41	-42.72	1.22
1.6	0.61	-59.22	13.63	4.80	126.78	-24.34	0.061	-15.00	0.41	-44.90	1.25
1.7	0.61	-62.73	13.54	4.75	123.96	-24.53	0.059	-15.44	0.40	-46.95	1.27
1.8	0.61	-66.34	13.45	4.70	121.14	-24.72	0.058	-15.78	0.39	-48.94	1.29
1.9	0.61	-69.85	13.36	4.66	118.37	-24.93	0.057	-16.07	0.39	-50.92	1.32
2	0.61	-73.41	13.27	4.61	115.53	-25.10	0.056	-16.19	0.38	-52.95	1.34
2.1	0.61	-76.93	13.19	4.57	112.76	-25.29	0.054	-16.23	0.37	-54.81	1.36
2.2	0.61	-80.55	13.10	4.52	109.97	-25.48	0.053	-16.15	0.37	-56.73	1.39
2.3	0.61	-84.18	13.02	4.48	107.22	-25.69	0.052	-16.20	0.36	-58.62	1.42
2.4	0.61	-87.95	12.95	4.44	104.46	-25.88	0.051	-16.12	0.36	-60.36	1.46
2.5	0.60	-91.46	12.87	4.40	101.71	-26.04	0.050	-15.93	0.35	-62.11	1.48
3	0.59	-109.93	12.46	4.20	88.05	-26.89	0.045	-13.42	0.33	-69.84	1.66
3.5	0.58	-128.36	12.02	3.99	74.65	-27.67	0.041	-8.35	0.32	-76.05	1.89
4	0.57	-146.55	11.56	3.79	61.39	-28.07	0.040	-0.44	0.30	-81.51	2.08
4.5	0.56	-164.07	11.10	3.59	48.43	-27.72	0.041	9.10	0.29	-87.17	2.11
5	0.55	179.17	10.60	3.39	35.70	-26.66	0.046	16.13	0.28	-93.37	1.99
5.5	0.55	163.86	10.09	3.19	23.34	-25.28	0.054	19.97	0.26	-101.07	1.81
6	0.55	148.85	9.58	3.01	11.08	-23.76	0.065	20.39	0.25	-111.19	1.62
6.5	0.56	134.84	9.01	2.82	-0.85	-22.33	0.076	17.75	0.24	-124.51	1.48
7	0.57	121.13	8.44	2.64	-12.44	-21.13	0.088	13.58	0.23	-137.46	1.38
7.5	0.58	108.36	7.85	2.47	-23.66	-20.03	0.100	9.01	0.23	-151.87	1.30
8	0.58	95.90	7.25	2.31	-34.68	-19.00	0.112	3.27	0.24	-165.58	1.22

Noise Parameters

Freq (GHz)	F_{min} (dB)	Γ_{opt} Mag	Γ_{opt} Ang	R_n/Z_o	G_a (dB)
0.5	1.46	0.32	10.51	0.37	16.5
0.8	1.49	0.31	21.95	0.35	16.3
0.9	1.50	0.31	28.21	0.34	16.19
1	1.51	0.3	32.89	0.34	16.1
1.1	1.52	0.3	39.85	0.33	16.0
1.5	1.57	0.29	45.05	0.30	15.61
1.8	1.60	0.28	50.05	0.28	15.2
1.9	1.61	0.28	57.75	0.27	15.02
2	1.62	0.27	59.67	0.27	14.9
2.1	1.63	0.27	63.12	0.26	14.8
2.2	1.64	0.26	64.28	0.26	14.65
2.3	1.65	0.26	68.3	0.25	14.58
2.4	1.66	0.25	75.25	0.24	14.48
2.5	1.68	0.25	78.03	0.24	14.39
3	1.73	0.23	94.06	0.21	13.98
3.5	1.78	0.21	121.52	0.18	13.39
4	1.84	0.2	141.87	0.16	12.9
4.5	1.89	0.21	172.98	0.15	12.45
5	1.94	0.24	-169.13	0.14	12
5.5	2.00	0.28	-146.48	0.16	11.59
6	2.05	0.31	-133.04	0.19	11.1

Appendix D

Calculating ΔT Using Microwave Office

To calculate the change in Noise Temperature using Microwave office, an S-parameter model for the antenna array was exported from FEKO to Microwave Office. A touchstone file containing the necessary parameters of the LNA was created and imported to Microwave Office, generating the LNA component block. An LNA was connected to each port of the antenna array and match terminated.

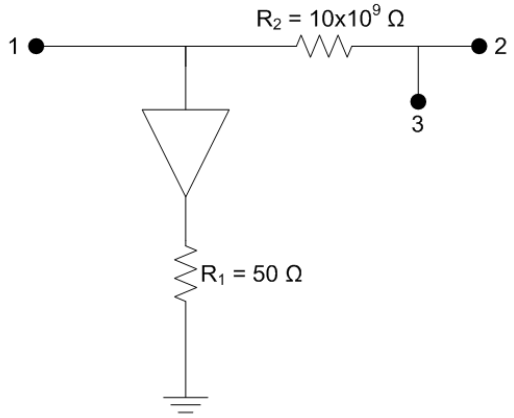

Figure D.1: Verification Port

The port model illustrated in Figure D.1 is the port model used to measure the added noise temperature due to noise coupling. The input port is connected to node 1, the output port is connected to node 2, and the array port to which

the added noise temperature due to noise coupling is calculated, is connected to node 3. Since R_2 effectively directs all current through the amplifier to ground, the noise temperature measured at the output port is only due to noise power coupled from other elements.

This calculation was repeated for every port of the antenna array. Figure D.2 illustrates the Microwave Office schematic used to calculate ΔT.

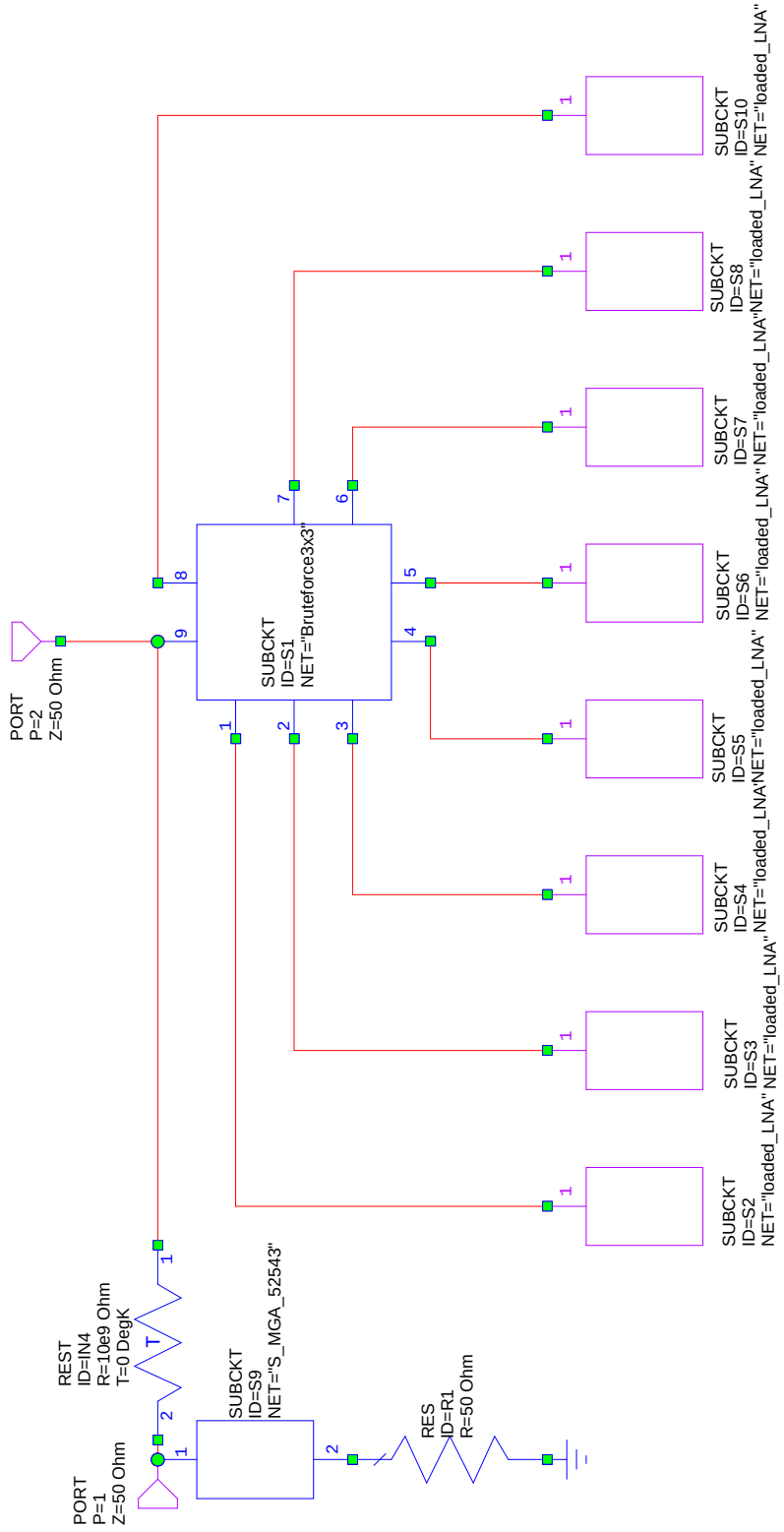

Figure D.2: Microwave Office Schematic

Bibliography

[1] Räisänen, Antti V. Lehto, Arto: *Radio Engineering for Wireless Communication and Sensor Applications*. Artech House, 2003.

[2] Haus, Hermann A. Melcher, James R.: *Electromagnetic Fields and Energy*. Prentice-Hall, 1989.

[3] Birney, D.S.: *Observational Astronomy*, pp. 278–295. 1st edn. Cambridge University Press, 1991.

[4] Burke, Bernard F. Graham-Smith, Francis: *An Introduction to Radio Astronomy*, pp. 367–373. 2nd edn. Cambridge University Press, 2002.

[5] Online. Last Accessed: August 2009.
Available at: `http://www.skatelescope.org`

[6] Carilli, C.L Rawlings, S: Science with the square kilometre array: Motivation, key science projects and assumptions. *New Astronomy Review*, pp. 979–984, December 2004.

[7] Online. Last Accessed: August 2009.
Available at: `http://www.ska.ac.za`

[8] Burke, Bernard F. Graham-Smith, Francis: *An Introduction to Radio Astronomy*, pp. 1–7. 2nd edn. Cambridge University Press, 2002.

[9] Kutner, M.L.: *Astronomy: A Physical Perspective*. 2nd edn. Cambridge University Press, 2003.

[10] Kitchin, C.R.: *Astrophysical Techniques*. 4th edn. Cambridge University Press, 2003.

[11] Verschuur, G.L.: *The Invisible Universe*, pp. 145–147. 2nd edn. Springer, 2006.

[12] Verschuur, G.L.: *The Invisible Universe*, pp. 4–11. 2nd edn. Springer, 2006.

[13] Burke, Bernard F. Graham-Smith, Francis: *An Introduction to Radio Astronomy*, pp. 8–20. 2nd edn. Cambridge University Press, 2002.

[14] Christansen, W.N. Hoegbom, J.A.: *Radiotelescopes*. 2nd edn. Cambridge University Press, 1987.

[15] Jeffs, Brian D. Warnick, Karl F. Landon, Jonathan Waldron, Jacob Jones, David Fisher, Richard Norrod, Roger D.: Signal processing for phased array feeds in radio astronomical telescopes. *IEEE Journal of Selected Topics in Signal Processing*, pp. 635–646, October 2008.

[16] Hay, S.G, O'Sullivan, J.D Kot, J.S Granet, C. Grancea, A. Forsyth, A.R. Hayman, D.H: Focal plane array development for askap (Australian Pathfinder). In: *The Second European Conference on Antennas and Propogation, 2007, EuCAP 2007*. November 2007.

[17] Bij de Vaate, J.G Ivashina, M.V: Focal plane arrays: Radio astronomy enters the ccd area. In: *International Union of Radio Science General Assembly*. October 2008.

[18] Weem, Jan Peeters Popovic, Zoya: A method for determining noise coupling in a phased array antenna. In: *IEEE MTT-S International Microwave Symposium Digest*, pp. 271–274. May 2001.

[19] Veidt, B.: Focal plane array architectures: Horn clusters vs. phased array techniques. February 2006. SKA memo 71.
Available at: `http://www.skatelescope.org/PDF/memos`

[20] Veidt, B. Dewdney, P.: A phased array feed demonstrator for radio telescopes. In: *International Union of Radio Science General Assembly*. 2005.

[21] Ivashina, M.V Simons, J Bij de Vaate, J.G : Efficiency analysis of focal plane arrays in deep dishes. *Experimental Astronomy*, vol. 17, pp. 149–162, 2004.

[22] Van Cappellen, W.A. Bij de Vaate, J.G Ivashina, M.V Bakker, L. Oosterloo, T.: Focal plane arrays evolve. In: *International Union of Radio Science XXIX General Assembly*. August 2008.

[23] DeBoer, David R. et al.: Australian ska pathfinder: A high-dynamic range wide-field of view survey telescope. In: *Proceedings of the IEEE*, pp. 1507–1521. August 2009.

[24] Ivashina, M. Ng Mou Kehn, M. Kildal, P. Maaskant, R.: Decoupling efficiency of a wideband vivaldi focal plane array feeding a reflector antenna. *IEEE TRANSACTIONS ON ANTENNAS AND PROPAGATION*, vol. 57, pp. 373 – 382, February 2008.

[25] Bhattacharyya, A.K.: *Phased Array Antennas*. 1st edn. Wiley, 2006.

[26] Balanis, C.: *Antenna Theory Analysis and Design*. Wiley, 2005.

[27] *FEKO User's Manual, Suite 5.4*. EM Software & Systems-S.A (Pty) Ltd, 1st edn, July 2008.

[28] Davidson, D.B.: *Computational electromagnetics for RF and microwave engineering*. 1st edn. Cambridge University Press, 2005.

[29] Nilsson, James W. Riedel, Susan A.: *Electric Circuits*. 7th edn. Pearson Prentice Hall, 2005.

[30] Zill, Denis G. Cullen, Micheal R.: *Advanced Engineering Mathematics*. Jones and Bartlett, 2000.

[31] Pahl, P.: Introduction to methods predicting the features of a finite phased array from an infinite one. Tech. Rep., University of Stellenbosch, 2008.

[32] Ziemer, Roger E. Tranter, William H.: *Principles of Communications*. 5th edn. Wiley, 2002.

[33] Brisken, W.: Focal plane arrays for the VLA? May 2004.
Available at: `http://www.astron.nl/other/pdf/Brisken FPAs for the VLA.pdf`

[34] Pozar, D.M.: *Microwave Engineering*. 3rd edn. Wiley, 2005.

[35] Weinreb, S.: Receiver tdp report to us ska consortium. May 2008. Available at: `http://skatdp.astro.cornell.edu/SKATDPDocuments.html`

[36] van der Walt, P.: Notes on antenna noise analysis, April 2009. Private Correspondence.

[37] Bahl, I.: *Fundamentals of RF and Microwave Transistor Amplifiers*. Wiley, 2009.